The microbiome of the pelagic tunicate Dolioletta gegenbauri: a potential link between the grazing and microbial food web

Tiago Pereira¹, Tina Walters², Hisham El-Shaffey³, Holly Bik¹, and Marc Frischer²

¹University of Georgia ²Skidaway Institute of Oceanography ³North Carolina State University at Raleigh

January 14, 2022

Abstract

Doliolids often form massive blooms during upwelling conditions in sub-tropical shelves. However, their trophic role, including their nutritious fecal pellets, in pelagic marine food webs remains poorly investigated. In this study, we performed three independent feeding experiments of cultured Dolioletta gegenbauri and used qPCR analysis and 16S rRNA metabarcoding to characterize the microbial community associated with full gut (FG) and empty (EG) doliolids, fresh (FP2Hrs) and senescing (FP24Hrs) fecal pellets, and the surrounding natural seawater (SW). Bacterial abundance (i.e., 16S rRNA gene copies) in EG samples was an order of magnitude lower than in SW and three orders lower than in FP24Hrs. Diversity analyses, based on the 16S rRNA metabarcoding data, supported a richer microbial community in SW, FP2Hrs, FP24Hrs, and FG samples. Furthermore, microbial community structure was determined by sample type, with FG samples appearing more similar to either FP2Hrs or FP24Hrs. These patterns resulted from the higher number of shared ASVs and consequently the contribution of similar major bacterial taxa (e.g., Rhodobacteraceae, Pirellulaceae). These observations support the hypothesis that there are significant ecological and trophic interactions between D. gegenbauri and the ocean microbiome. Predicted gene function recovered many genes related to key processes in the marine environment and supported greater similarity between FP2Hrs, FP24Hrs, and FG samples. These observations suggest that pelagic marine bacteria are utilized by D. gegenbauri to digest captured prey particles, and the subsequent release of fecal pellets supports the rapid proliferation of distinct microbial communities which likely influence key biogeochemical processes in the ocean.

1 INTRODUCTION

Marine gelatinous zooplankton, including the mucus-feeding pelagic tunicates (e.g., appendicularia, pyrosomes, salps, and doliolids), occur circumglobally and play a central role in marine planktonic food webs (Alldredge & Madin, 1982; Conley, Lombard, & Sutherland, 2018; Frischer et al., 2021). However, understanding their role in marine pelagic systems remains limited primarily due to methodological challenges that constrain the ability to sample and culture them, (Alldredge & Madin, 1982; D. Deibel & Paffenhofer, 2009; Takahashi et al., 2015). Pelagic tunicates have long been considered intriguing components of marine pelagic systems due to their ability to form large blooms. For example, pelagic tunicate blooms may decouple grazing linkages between the mesozooplankton and higher trophic levels (Sullivan & Kremer, 2011) and impact the vertical export of carbon to depth and biogeochemical cycling (Lebrato, Pahlow, Frost, & Küter, 2019; Richardson, 2019). More recently, it has been suggested that mucus feeding pelagic organisms, and specifically the doliolid *Dolioletta gegenbauri*, participate in a complex relationship with microbial communities that potentially impact the composition and activity of the ocean microbiome (Frischer et al., 2021).

Doliolid blooms are common features of sub-tropical continental shelves and oceans (Bone, 1998). Fundamentally, as is the case for other zooplankton groups, doliolid blooms result from the delivery of nutrients into the euphotic layer by a variety of physical mechanisms that result in increased phytoplankton production (Boero et al., 2008). Although the specific mechanisms contributing to doliolid bloom formation remain unclear, the presence of fine-scale oceanographic boundaries, including vertical pycnoclines and horizontal fronts, appears to be an important factor (Greer et al., 2020; B. Martin, Koppelmann, & Kassatov, 2016; Takahashi et al., 2015). The ecological significance of doliolid blooms, however, can be highly variable and dependent on the location, duration, and blooming species. Because doliolids are efficient filter feeders (Don Deibel & Paffenhöfer, 1988: Ishak et al., 2020: Takahashi et al., 2015) and produce low-density fecal pellets with slow sinking rates (Don Deibel, 1990; Patonai, El-Shaffey, & Paffenhöfer, 2011), it is believed that they have the potential to significantly influence shelf carbon cycling, pelagic ecology, and pelagic-benthic coupling (Don Deibel, 1985; Ishak et al., 2020). To our knowledge, however, their influence on the ocean microbiome and microbially-mediated processes has not been carefully explored. While it is increasingly recognized that blooms of large gelatinous organisms (e.g., scyphomedusae) influence marine microbial assemblages by releasing large amounts of mucus (Condon et al., 2011; Hao, Gerdts, Holst, & Wichels, 2019; Lebrato et al., 2019; Winder et al., 2017), less is known about the interaction between doliolids and microbial processes. The link between doliolids and pelagic microbial communities, however, is potentially more fundamental to ecosystem functioning due to their much higher abundances relative to scyphomedusae (Greer, Chiaverano, Treible, Briseño-Avena, & Hernandez, 2021; Takahashi et al., 2015; Walters et al., 2019) and production of microbially-labile fecal pellets.

Doliolids undergo a complex life cycle that alternates between sexual and asexual stages (Walters et al., 2019). Moreover, changes in size and feeding preference are likely to influence their trophic role and relevant ecological interactions. Given both the size range of particles captured and the release of high organic content pellets, the doliolid life cycle is likely coupled to the microbial food web and the myriad of microbially-mediated processes responsible for the cycling of carbon in shelf systems. As with all pelagic tunicates, doliolids are efficient filter feeders and can clear large volumes of water in both low- and high-food concentration environments (Lucas & Dawson, 2014). Based on anatomical considerations, laboratory-based experimental studies, and inferred from field observations, doliolids are capable of ingesting particles over a wide size range from less than a micron (bacteria) to 100's of microns but optimally between $1-50 \ \mu m$ (Don Deibel, 1985; Tebeau & Madin, 1994). Historically, because of their feeding mechanism, doliolids were assumed to be passive grazers, non-selectively capturing particles that they encounter (Crocker, Alldredge, & Steinberg, 1991; Vargas & Madin, 2004). More recently, however, using molecular gut content analysis and stable isotope tools applied to cultured and wild-caught doliolids, it has been recognized that doliolids are capable of selective feeding and that a significant portion of their diet is likely derived from microbialprocessed detrital material (Frischer et al., 2021; Walters et al., 2019). The importance of detrital material and fecal pellets in the doliolid diet further implies a close relationship between the host-associated doliolid microbiome and the broader ocean microbiome.

Zooplankton microbiome investigations are relatively rare and have primarily focused on copepods that generally dominate marine zooplankton communities. Copepod microbiomes contain diverse and abundant bacterial communities (Datta et al., 2018; De Corte et al., 2018; Moisander, Sexton, & Daley, 2015; Shoemaker, Duhamel, & Moisander, 2019; Tang et al., 2019) that differ significantly from bacterial communities associated with the surrounding seawater. These studies suggest that crustacean zooplankton-associated bacterial communities are likely shaped by host species. Similarly, in the few studies that have examined microbiomes associated with gelatinous zooplankton, host microbiomes differed from the surrounding water; however, unlike copepods, the diversity of microbiomes associated with gelatinous zooplankton appears to be very low (Daniels & Breitbart, 2012; Jaspers et al., 2020; Tinta et al., 2019; Viver et al., 2017). In freshwater systems, Eckert et al. (2021) reported that the microbiomes from a diversity of zooplankton groups (e.g., rotifers, cladocerans, and copepods) were more similar to the surrounding water microbiome, and the authors concluded that the environment rather than the host largely shaped the composition of zooplankton associated bacterial communities.

To our knowledge, the doliolid microbiome has not previously been investigated, and it is unknown whether doliolids possess a stable endemic core microbiome or a transient environmentally dependent microbiome. Similarly, many ecologically relevant questions pertaining to doliolid/microbial interactions exist. Because doliolids can produce buoyant organic-replete fecal pellets and are efficient at capturing particles it is hypothesized that they may significantly impact the microbial activity and composition in the surrounding water column. In this study, we utilized cultured *D. gegenbauri* zooids exposed to freshly collected natural seawater containing native microbial communities in order to investigate the composition of microbiomes associated with doliolids, doliolid fecal pellets, and the surrounding ocean waters to explore the hypothesis that the doliolid and ocean microbiome are intricately interdependent.

2 MATERIALS AND METHODS

2.1 Doliolid feeding experiments

To explore the hypothesis that the doliolids and ocean microbiome are intricately interdependent, three independent feeding experiments (Exp1: January/2016, Exp2: March/2016, Exp3: April/2016) were conducted with D. gegenbauri gonozooids reared under optimal cultivation conditions as previously described (Walters et al., 2019). Thus, the initial seawater (SW) containing the native microbial communities differed among experiments, especially between experiments 1 and 2-3 (i.e., experiments 2 and 3 were performed a month apart). To estimate the microbial community composition in the environment, SW samples were collected at the start of each feeding experiment. Briefly, near-bottom seawater was prefiltered through a 63 µm sieve and 150 mL collected in triplicate onto a 25 mm 0.2 µm Supor filter (PALL Life Sciences, East Hills, NY, USA). The filter was placed in a sterile 2 mL cryovial and stored at -80°C until DNA was extracted. To initiate feeding experiments, 15 laboratory-reared D. gegenbaurigonozooids were transferred to 1.9 L glass jars that contained freshly collected near-bottom seawater and acclimatized for 2 hr on a rotating plankton wheel (ca. 0.3 rpm) to keep them in constant suspension. Following acclimation, doliolids were transferred to fresh near-bottom seawater in 1.9 L jars and allowed to feed for 2 hr. Assuming average gut residence times of 20–30 min and clearance rates of 0.5–1 L/day (Gibson, D. M., 2000), during the 2 hr feeding period the doliolids would have been expected to have cleared 250-700 mL (13%-35%) of the feeding vessel volume during the experimental period.

After the feeding period, doliolids (FG: full gut samples) were immediately removed from the feeding chamber and anesthetized by placing them into 0.2 μ m filtered seawater containing 0.4% MS-222 (3-aminobenzoic acid ethyl ester; Alfa Aesar). After the animals had been anesthetized, they were individually rinsed 3 times in 0.2 μ m filtered seawater containing MS-222 and transferred to individual 2 ml tubes containing extraction buffer ATL from the DNeasy Blood and Tissue kit (Qiagen, Valencia CA, USA). For empty gut (EG) samples, doliolids were kept in 0.2 μ m filtered seawater and starved for a period of 24 hrs. Previous studies showed that after this period prey items are no longer detected in the doliolid gut (Walters et al., 2019).

In addition to FG and EG samples, freshly (FP2Hrs) and aged (FP24Hrs) fecal pellets produced by feeding doliolids were collected during the experimental period. The remaining gonozooids were transferred to two 1.9 L jars containing 10 μ m filtered near-bottom seawater and allowed to produce fecal pellets for a period of 2 hr. Following the 2 hr incubation period, half of the fecal pellets (FP2Hrs) were immediately collected while the remaining pellets were allowed to incubate for 24 hr (FP24Hrs). Fecal pellets were collected by centrifugation at 500 x g for 5 min after they were rinsed 3 times in 0.2 μ m filtered seawater. The pellets were transferred to 2 mL tubes containing extraction buffer ATL. Tracing of fecal pellets for a period longer than 24 hrs was not feasible due to degradation. All samples were stored at 4°C until DNA was extracted, usually within 24–48 hr after initial collection.

2.2 DNA extraction, PCR, and Illumina sequencing

Genomic DNA from doliolids (EG and FG), fecal pellets (FP2Hrs and FP24Hrs), and seawater (SW) samples were extracted using the Qiagen DNeasy Blood & Tissue kit (Qiagen, Valencia CA, USA) following the manufacturer's instructions and as previously described in Walters et al. (2019). Following extraction, purified DNA extracts were quantified using a Qubit \mathbb{R} 2.0 Fluorometer with the dsDNA HS assay reagents (ThermoFisher Scientific). Yields ranged from 40 to 254 ng (0.20 to 1.3 ng/µL) DNA gonozooid⁻¹ and 0.26

to 0.49 ng/µL DNA per 100 mL of water. DNA samples were archived and stored at -20°C until further analysis. A total of 37 DNA extracts representing FG, EG, FP2Hrs, FP24Hrs, and SW sample types from three experiments were collected throughout this study.

DNA extracts from *D. gegenbauri* (EG, FG), fecal pellets (FP2Hrs and FP24Hrs), and seawater (SW) samples were used to amplify (in triplicate) the 16S rRNA gene from bacteria/archaea using the updated primers 515F (Parada, Needham, & Fuhrman, 2016) and 806R (Apprill, McNally, Parsons, & Weber, 2015) targeting the V4 region. Dual-index primer constructs were designed by modifying the Earth Microbiome Project (EMP) Illumina amplicon protocol (Thompson et al., 2017). A second barcode region was added to reverse 16S rRNA PCR primers. All primer constructs and oligo sequences have been made available on FigShare (*https://doi.org/10.6084/m9.figshare.5701090*). The amplification of the 16S rRNA gene was performed using the reagents and PCR conditions in the EMP protocols (Caporaso et al., 2012).

PCR reactions had a final volume of 25 μ L and contained 1 μ L of DNA template, 0.5 μ L of each primer (10 μ M), 10 μ L of Platinum Hot Start PCR Master Mix (2x) (Thermo Fisher), and 13 μ L of molecular-grade water. Both positive (ZymoBIOMICSTM Microbial Community Standard; Zymo Research, Irvine, CA) and negative (molecular-grade water, HyClone HyPure Water, GE, Healthcare Life Sciences) controls were included in all PCRs. The following PCR profile was used for amplification of the 16S rRNA gene fragment: 94°C for 3 min; 94°C for 45 s, 50°C for 60 s and 72°C for 90 s for 35 cycles; and 72°C for 10 min. PCR amplification success was evaluated with gel electrophoresis (agar 1%) to confirm gel bands of the expected fragment size. Purification of PCR products was subsequently carried out using a magnetic bead purification protocol using Agencourt AMPure XP beads (Beckman Coulter, CA, USA) and following the manufacturer's protocol. Additional details on PCR conditions (e.g., sterilization) are provided in Schuelke et al. (2018).

After PCR cleanup, sample concentrations were measured using a Qubit ($\mathbf{\hat{R}}$ 3.0 Fluorometer with the dsDNA HS (High sensitivity) Assay Kit (Thermo Fisher Scientific) and normalization values were calculated to ensure that approximately equivalent DNA concentrations were pooled across all samples. After pooling, the library was subjected to a final magnetic bead cleanup step, followed by size selection on a BluePippin (Sage Science, Beverly, MA) to remove any remaining primer dimer and isolate target PCR amplicons within the range of 300–700 bp. A Bioanalyzer trace was run on the size-selected pool as a quality control measure, and the 16S rRNA library (115 samples in total, including 2 negative and positive controls) was sequenced on the Illumina MiSeq Platform (2 x 300-bp paired-end run) at the UC Davis Genomics Core Facility (Schuelke, Pereira, Hardy, & Bik, 2018). All wet laboratory protocols and downstream bioinformatics scripts used in this study have been deposited on GitHub (*https://github.com/BikLab/doliolids*).

2.3. Quantitative polymerase chain reaction (qPCR) assay

Microbial DNA concentrations associated with EG, FP24Hrs, and SW sample types from the feeding experiments were estimated by real-time qPCR using a Bio-Rad CFX96 Real-Time PCR System (Bio-Rad Laboratories, Hercules, California). Primers used in this study included the universal 16S rRNA primers 932F (CGCACAAGCRGYGGAGYATGTG) and 1062R (CACRRCACGAGCTGACGA) which generated amplicons < 200 bp (Allen et al., 2005). qPCR reactions were performed in 20 μ L reactions containing a final concentration of 1X SsoFast EvaGreen (R) Supermix (Bio-Rad Laboratories, Hercules, California), 0.3 μ mol of each primer, and 1 μ L genomic DNA per reaction. Quantitative standard curves were generated from a 6-order of magnitude serial dilution of plasmid DNA (pDNA) containing a cloned copy of the target 16S rRNA gene (*E. coli*) ranging from 10¹ to 10⁷ target gene copies per reaction. qPCR cycling conditions included an initial enzyme activation step at 95 °C for 30 s followed by 45 cycles of denaturation (95 °C, 5 s) and annealing/extension (54.7 °C, 5 s). After cycling, product melt temperatures were evaluated from 60 to 95 °C at 0.5 °C increments for 5 s each. Samples, standards, and no-template controls were assayed in triplicate.

2.4 Bioinformatics and statistical analyses

Raw Illumina data were demultiplexed using a custom script for handling dual-index barcode combinations

(available on GitHub:https://github.com/BikLab/doliolids). The demultiplexed 16S rRNA dataset was analyzed in QIIME2 version 2020.11 (Bolyen et al., 2019) where the primer and adapter sequences were trimmed using the cutadapt plugin (M. Martin, 2011). An error rate of 0.1 was allowed; reads were discarded when no adapter/primer sequences were found. Denoising was based on optimal parameters (forward and reverse reads truncated at 237 and 253 bp, respectively; median PHRED score of [?]30). Subsequently, Amplicon Sequence Variants (ASVs) were estimated using the DADA2 algorithm, which is based on a 100% sequence identity [i.e., single-nucleotide resolution; (Callahan et al., 2016)].DADA2 was run using default parameters, including default chimera checking parameters (consensus option, which carries out de novo chimera identification and removes ASVs identified as chimeras). Taxonomy assignments for ASVs were obtained using a combination of the BLAST+ consensus taxonomy classifier [minimum confidence value of 0.8; (Camacho et al., 2009)] and the SILVA 138 SSURef NR99 release (Quast et al., 2013), and through the SILVAngs tool using the same SILVA release and the default parameters, except for sequence identity which was set to 1.0 (Quast et al., 2013).

The final dataset consisted of 115 samples (FG: 39, EP: 39, FP2Hrs: 9, FP24Hrs: 12, SW: 12, PCR controls: 4). Except for PCR negative controls, all other samples had high sequence depth (> 2,000 reads, Table S1, Appendix S1). Preliminary analyses showed that ASVs found in PCR controls were not, in its great majority, shared by experimental samples (Fig. S1, Appendix S2). Nevertheless, the R package *decontam* was used to assess the levels of contamination in our dataset by implementing the prevalence method with a threshold of 0.5 (Davis, Proctor, Holmes, Relman, & Callahan, 2018). Sequences determined to be contaminants (a total of four ASVs) were removed from the dataset and the resulting ASV table was summarized and analyzed to assess patterns of microbial community variation associated with sample types (i.e., FG, EG, FP2Hrs, FP24Hrs, and SW) across the different experiments (i.e., Exp1, Exp2, and Exp3).

For each sample type, the total number of demultiplexed and quality trimmed reads, the number of reads and ASVs retained by DADA2 as well as after contaminant filtering with *decontam* were calculated (Table S1, Appendix S1). Diversity estimates including Observed diversity (i.e., number of ASVs), Shannon diversity H' (Log₂), Inverted Simpson (D) diversity, and Pielou's Evenness (J') were extracted from the filtered ASV tables using the package *phyloseq*(McMurdie & Holmes, 2013), and compared among sample types for each experiment separately. Data normality was assessed using Shapiro–Wilk's method, and Kruskal–Wallis (K-W) tests were used to assess differences among sample types with the package *FSA* v0.8.24 in R version 4.1.2 (R Core Team, 2021). The Mann–Whitney U test with adjustments for p-value [BH method; (Benjamini & Hochberg, 1995)] was used for pairwise comparisons (Zar, 2010). Alpha diversity was also explored with barplots based on the relative abundance of the most dominant taxa at different taxonomic levels (e.g., phylum, class, and order).

For each experiment, multivariate analyses were also performed at the level of ASVs. To visualize the similarity of microbial communities associated with the different sample types, a similarity matrix based on Bray-Curtis similarity and ASV-transformed abundances (i.e., standardized by total and square root transformed) was constructed. Ordination was done by Non-parametric Multidimensional Scaling (nMDS) and Goodness-of-fit given by the stress value (Clarke, 1993). The Permutational Analysis of Variance (PERMANOVA) was used to test for significance among sample types (Anderson, Gorley, & Clarke, 2008).

Differential abundance analyses were performed independently for each experiment using the R package ALDEx2 (v1.12.0) (Fernandes, Macklaim, Linn, Reid, & Gloor, 2013; Fernandes et al., 2014). ASV counts were transformed using a centered-log ratio (CLR) transformation for a compositionally coherent inference and estimates. Significant differences (p < 0.05) among sample types (EG, FG, F2Hrs, F24Hrs, and SW) were assessed through K-W tests at each taxonomic rank (i.e., from phylum to genus), also analyzed independently. False discovery rates (FDRs) were estimated using the Benjamini-Hochberg procedure (Benjamini & Hochberg, 1995). A heatmap depicting the differential abundance of microbial taxa that varied among sample types having microbial taxa at each level (rows) and samples (columns) was produced for each experiment. The *PICRUSt2* method was also used to predict potential gene functions from microbial community profiles associated with the different sample types (Douglas et al., 2020). Differential abundance analyses

on the matrices of predicted gene functions were performed and visualized as described above. Additionally, predicted gene functions were organized into distinct metabolic pathways following Yilmaz et al. (2015). For this study, all visualizations were produced with *ggplot2* v.3.1.1 in R (Wickham, 2016).

3 Results

3.1 qPCR analysis

Bacterial abundance, as inferred from 16S rRNA gene copy abundance, was assessed by quantitative PCR (qPCR) and normalized to sample volume. Unsurprisingly, in FP 24Hrs, the abundance of bacterial rRNA gene copies was at least two orders of magnitude higher than found in SW $(8.0+-7.1\times10^5 \text{ vs } 1.3+-1.8\times10^3 \text{ copies mm}^{-3})$ indicating that fecal pellets support the rapid proliferation of bacterial communities. However, the abundance of 16S rRNA copies was surprisingly an order of magnitude lower in EG samples compared to the water column on a per-volume basis $(0.05+-0.01\times10^3 \text{ copies mm}^{-3})$, Fig. S2, Appendix S2).

3.2 Sequencing depth and diversity estimates across sample types

The total number of reads retained for the filtered datasets (i.e., after *DADA2* and *decontam* procedures) was 1.5-2.3 times higher for experiments 2 and 3, respectively, when compared to experiment 1 (Exp1: 774,579, Exp2: 1,773,326, Exp3: 1,169,003; Table S1, Appendix S1). However, similar values were observed across all three experiments when considering the mean number of reads, (Exp1: 32,274, Exp2: 38,518, Exp1: 27,833). Significant differences for the number of reads among sample types were only observed in experiments 1 and 3, where EG samples displayed the lowest values (although not significantly different from FG in Exp1, Table S2, Appendix S1).

A summary of comparisons across sample types for the number of reads and different diversity estimates, per experiment, is given in Figure 1 and Table 1. Although a slight variation in sequence depth, and consequently in the mean number of reads, was observed across experiments, the mean number of AVSs (i.e., Observed diversity) was consistent with *DADA2* recovering 139, 144, 145 AVSs for experiments 1, 2, and 3, respectively (Table S1, Appendix S1). Nevertheless, significant differences among sample types were also detected for the number of ASVs in all three experiments (Fig. 1). Once again, lower values were always observed for EG samples, although not significantly different from FG samples in experiment 1 (Table S2, Appendix S1).

When analyzing the number of unique ASVs per sample type, a similar pattern is observed across experiments (Fig. S3, Appendix S2). Full gut doliolids always displayed the highest number of unique AVSs followed by either EG (Exp1 and Exp3) or SW (Exp2) samples, whereas FP2Hrs and FP24Hrs presented the lowest values. The number of ASVs shared among all sample types was consistent across experiments and relatively low, about 20-30% of the total number of ASVs (Exp1: 35, Exp2: 30, Exp3: 44). In experiments 1 and 3, the highest number of shared AVSs was observed between FG and FP2Hrs or between FG and FP24Hrs samples (26 and 79 AVSs, respectively), whereas in experiment 2, the highest number (55 AVSs) was observed between FG and FP24Hrs samples (Fig. S3, Appendix S2). When focusing on specific sample types, the highest number of shared AVSs, including all three experiments, was observed in SW (56 AVSs) followed by FG and FP24Hrs (both with 41 ASVs), whereas the lowest (29 AVSs) was found in EG samples (Fig. S4, Appendix S2).

Interestingly, nine out of the 29 ASVs exclusively found in EG samples were also consistently (i.e., frequency of [?] 50%) recovered in all three feeding experiments (Fig. 2; Table S3, Appendix S1). The recovery of such AVSs, which also represented different bacterial taxa, may suggest that doliolids have a core microbiome. Among these potential core taxa, *Pseudoalteronomas* and *Shimia* were the most abundant, especially in experiment 2. Yet, *Pelagibaca* and *Alteromonas*, in addition to being abundant, were the most frequent taxa, the latter recovered in all EG samples (Table S3, Appendix S1).

The highest mean values for diverse estimates were frequently found in SW samples whereas the lowest was in EG, except for experiment 1 (Table 1). In this case, FG samples showed the lowest values for most of the indices while FP24Hrs had the highest values for Observed and Simpson diversity indices. For Pielou's evenness, less variation was observed among sample types; whereas the highest mean values were

also observed in SW samples, lowest mean values were either found in FG samples (Exp1) or EG samples (Exp2 and Exp3). Moreover, in experiments 2 and 3 FP2Hrs and FP24Hrs samples presented similar values of alpha-diversity compared to those observed in SW and FG samples.

According to the KW analysis, significant differences (p<0.05) among sample types were detected for all the diversity indices in all three experiments (Table 1). Pairwise comparisons revealed that in experiment 1 FG samples were significantly different from all other sample types, except EG (Number of ASVs) and FP2Hrs (evenness). Still, in experiment 1, pairwise comparisons confirmed that SW, FP2Hrs, and FP24Hrs had similar alpha-diversity values (p>0.05), except for Simpson diversity (FP24Hrs significantly greater than SW; Table S2, Appendix S1). In experiments 2 and 3, EG samples had significantly lower values for all alpha-diversity indices when compared to the other sample types, except for evenness in experiment 3. Significant differences were also detected among other sample types, particularly concerning the number of AVSs (experiments 2 and 3) and Simpson diversity (experiment 2 only). Similar alpha-diversity values (p>0.05) were also observed for SW, FP2Hrs, FP24Hrs, and FG samples in experiment 3 (except for ASV numbers), thus suggesting a similar level of diversity among these sample types (Table S2, Appendix S1).

3.3 Microbial community structure and differences among sample types

Regardless of the experiment, microbial communities were always structured by sample type, that is, samples representing the same treatment tended to group together (Fig. 3). For example, the least diverse EG samples clearly separated from the other sample types, especially in experiments 2 and 3, suggesting that EG samples have a more dissimilar microbial community. The level of separation among FG, FP2Hrs, and FP24Hrs samples also varied according to the experiment. Accordingly, these sample types were: (i) clearly separated in experiment 1; (ii) relatively more similar (i.e., lower distances) in experiment 2; (iii) and showing some degree of overlap in experiment 3 (i.e., FG and FP24Hrs sample types). Seawater samples also differed substantially from all other sample types, particularly in experiments 2 and 3.

The PERMANOVA analysis confirmed that the associated microbial community significantly differed among sample types, and that was the case for all three experiments (Table S4, Appendix S1). Although significantly different, the degree of dissimilarity among sample types also varied. For example, the analysis of average similarity showed that higher similarity values were always found between FP2Hrs and FP24Hrs sample types (52.7-54.8%), regardless of the experiment. Conversely, the lowest similarity values were either observed between SW and FG sample types (Exp1: 10.2%) or between SW and EG sample types (Exp2: 2.9%, Exp3: 9.1%). The analysis of average similarity also showed that the microbial communities of FG and SW samples were more similar to that found in FP2Hrs or FP24Hrs. However, these values were often higher between FG and fecal pellets than between SW and fecal pellets (Table S4, Appendix S1).

3.4 Major microbial taxa associated with the different sample types

At the phylum level, the microbial communities associated with the different sample types were dominated by four (out of 37 phyla) major groups including *Proteobacteria*, *Cyanobacteria*, *Planctomycetota*, and *Bacteroidota* (Fig. 4A; Fig. S5, Appendix S2). In experiment 1, microbial communities were highly dominated by *Proteobacteria* ([?] 74%) followed by *Bacteroidota*, whereas in experiments 2 and 3, in addition to *Proteobacteria* (e.g., Exp2: 15-95%, Exp3: 26-86%), a greater contribution of *Cyanobacteria* (Exp2: 23-59%, Exp3: 19-29%) and *Planctomycetota* (Exp2: 11-23%, Exp3: 34-38%) is observed, except in EG samples. At the same time, a lower contribution of *Bacteroidota* is observed in experiments 2 and 3, except in SW samples (Exp2: 14%, Exp3: 12%).

At the order level, a greater variation of microbial communities across sample types and experiments is observed. For example, microbial communities were represented by: (i) *Pseudomonales* (25-63%) and *Rhodobacterales* (10-37%), both *Proteobacteria*, in experiment 1; (ii) *Synechococcales* (*Cyanobacteria*; 22-58%) and *Rhodobacterales* (5-46%) in experiment 2; (iii)*Synechococcales* (19-28%) and *Pirellulales*(*Planctomycetota*; 29-31%) in experiment 3 (Fig. 4B). The presence of SAR11 was primarily observed in SW samples, especially in experiments 2 and 3 (21% and 38%, respectively). Yet, *Enterobacterales* (*Proteobacteria*) was mostly found in EG (32-46%) and FP24Hrs (21-25%) sample types with very similar

abundances across all three experiments with the highest contribution of *Enterobacterales* observed in EG of experiment 2 (Fig. 4B).

When microbial communities are examined at the family and genus level, greater differentiation among sample types as well as between experiments 1 and 2-3 is observed (Fig. 5A-B). For example, EG and FP24Hrs sample types in experiment 1 were dominated by the *Proteobacteria* genus *Alteromonas* (Alteromonadaceae: 30% and 18%, respectively); FG and FP2Hrs samples by an uncharacterized *Rhodobacteraceae* genus (33% and 24%, respectively), and SW samples by the *Porticoccaceae* strain C1-B045 (29%), both taxa belonging to *Proteobacteria* (Fig. 5A-B).

Although experiments 2 and 3 showed relatively similar microbial profiles at the family level (Fig. 5A), including a high abundance of *Cyanobiaceae* (Exp2: 22-58%, Exp3: 19-28%) across all sample types (except EG) and dominance of *Pseudoalteromonadaceae* in EG samples (Exp2: 44%, Exp3: 29%), trends specific to each experiment and sample type were also detected when assessing the contribution of different bacterial genera. For example, *Cyanobium* (8-24%) and *Synechococcus* (14-32%), both *Cyanobiaceae*, dominated FG, FP2Hrs, and FP24Hrs sample types in experiment 2. Yet, in experiment 3, in addition to *Cyanobium* (12-21%), *Blastopirellula* (10%;*Pirellulaceae*), *Synechococcus* (6-7%), and*Rubripirellula* (13-14%; *Pirellulaceae*) were also abundant in the same sample types (Fig. 5B).

The microbial profile of SW samples in experiments 2 and 3 was very similar (i.e., same taxa and with similar contribution) and included, in addition to some of the above-mentioned taxa, representatives of the SAR11 Clade 1a (Exp2: 16%, Exp3: 26%). Moreover, SW samples were characterized by many low abundance taxa (greater percentage of "Others", Fig. 5B). Some unique differences among experiments included the presence of *Leoginellaceae* taxa in experiment 1 (FG, FP2Hrs, and to a lesser extent FP24Hrs), the contribution of the *Proteobacteria Shimia* (*Rhodobacteraceae*) in experiment 2, especially in EG samples (up to 42%), and the relatively high abundance of the *Proteobacteria Marinomonas*(*Marinomonadaceae*, 21%) in EG samples of experiment 3. Overall, the assessment of the microbial community composition across sample types at different taxonomic ranks supported the patterns observed in both alpha and beta diversity analyses. In this sense, SW, FG, FP2HRs, and FP24HRs samples show a more diverse (and somewhat similar) microbial community when compared to EG samples (Figs. 1 and 2).

3.5 Differential abundance analysis of microbial taxa

In this study, a large number of microbial taxa was observed, especially in SW samples, including some that were differentially abundant (p<0.05) across sample types (Fig. 6; Table S5, Appendix S1). This number increased as the taxonomic resolution increased, and it was particularly higher in experiments 2 and 3 when compared to experiment 1. A summary of the differentially abundant taxa across sample types for each experiment, including their read count and relative abundance, is presented in Appendix S1 (Table S5). In experiment 1, 13 phyla were differentially abundant (7 after FDR with BH) whereas 21 and 19 phyla were recovered from experiments 2 and 3, respectively.

Planctomycetota was the most differentially abundant taxa across sample types in all three experiments (i.e., ranked in 1) and it was consistently more abundant in FP2Hrs, FP24Hrs, and FG samples. The SAR324 MG-B group was also important in SW samples of all three experiments (ranked in 5, 10, and 12, respectively), whereas *Thermoplasmota* (ranked in 13 and 15), *Marinimicrobia*(ranked in 15 and 16), and *Bacteroidota* (ranked in 8 and 6, respectively) were only important in SW samples of experiment 2 and 3. Conversely, *Acidobacteriota* was differentially abundant only in experiment 1, being more abundant in EG and FG samples. *Cyanobacteria* were differentially abundant in all three experiments (ranked in 4, 2, and 2, respectively) and particularly important in FP2Hrs and FP24Hrs as well as FG samples (only in experiment 2 and 3).

At the genus level, 115, 170, and 131 taxa were differentially abundant across sample types in experiments 1, 2, and 3, respectively (85, 105, and 78 after FDR with BH method). Based on these differently abundant taxa genera (lowest taxonomic rank in the present study), it is observed that some sample types displayed a similar pattern with respect to their abundance. For example, FP2Hrs, FP24Hrs, and to a lesser extent

FG, displayed similar patterns of differentially abundant taxa, especially in experiment 3. Alteromonas was important in EG samples and differentially abundant in experiments 1 and 2 (ranked in 2 and 3) but not in experiment 3. Cyanobium PCC-6307 was differentially abundant in all three experiments (ranked in 68, 1, and 5, respectively) and relatively important across all sample types in experiments 2 and 3 (except for EG samples). On the other hand, some differentially abundant taxa were specific to a sample type and experiment. For example, the genus Alcanivorax and an uncharacterized genus of the SAR202 group (Dehalococcoidia) were only differentially abundant in experiment 1 and relatively important in EG and SW samples, respectively (Fig. 6).

3.6 Predicted functional genes associated with doliolids and other sample types

Predictions of functional potential using PICRUSt2 resulted in a large number of gene families (i.e., EC number in our study). These were further reduced based on the differential abundant analysis with ALDEx2. Accordingly, 1659, 1668, and 1651 predicted gene functions were differently abundant across sample types in experiments 1, 2, and 3, respectively (Table S6, Appendix S1). Moreover, the most abundant (e.g., top 20) predicted functions were highly consistent across sample types and experiments. For example, in all three experiments, the most abundant predicted function across all sample types was a transferase (EC:2.7.7.7 - DNA-directed DNA polymerase), except for a hydrolase (EC:3.6.4.12 - DNA helicase) in FP2Hrs of experiment 2. The contribution of EC:2.7.7.7 was highest (always > 1%) in SW, EG, and FG for experiments 1, 2, and 3, respectively (Table S6, Appendix S1).

When solely focusing on the most differentially abundant predicted functions across sample types, FP2Hrs, FP24Hrs, FG, and to a lesser extent SW samples, tend to display similar patterns (i.e., high abundance for the same predicted functions), especially in experiments 1 and 2. Conversely, in experiment 3, EG and FP24Hrs samples displayed relatively similar patterns concerning predicted functions, except for an oxidoreductase (EC:1.13.11.11 - tryptophan 2,3-dioxygenase), more abundant in the former group. A summary of the 20 most differentially abundant predicted gene functions for each experiment is given in Figure 7 (see Table S6, Appendix S1 for additional details).

In experiment 1, some of the highly differentially abundant predicted functions included the 5-dehydro-4-deoxy-D-glucuronate isomerase (EC:5.3.1.17, Isomerase, rank19), Carboxynorspermidine decarboxylase (EC:4.1.1.96, Lyase, rank 16), and Nicotinamide phosphoribosyltransferase (EC:2.4.2.12, Transferase, rank 15) which were more important in FG24Hrs samples. The most differentially abundant predicted function in experiment 1, Uronate dehydrogenase (EC:1.1.1.203, Oxidoreductase, rank 1), was important in all sample types, except EG samples. Although an overall agreement is observed with respect to the predicted functions between FG, FP2Hrs, and FP24Hrs, there were also cases where SW was more similar to fecal pellet samples (e.g., EC:2.7.1.31 - Glycerate 3-kinase, EC:2.3.1.31 - Homoserine O-acetyltransferase; Fig. 7).

In experiment 2, those included All-trans-zeta-carotene desaturase (EC:1.3.99.26, Oxidoreductase, rank 19) and N-acetylmuramoyl-L-alanine amidase (EC:3.5.1.28, Hydrolase, rank 3) especially more abundant in SW samples, but also recovered in FG and fecal pellets. Overall, consistent results with experiment 1 were observed, where the same predicted functions (i.e., among the 20 most differentially abundant ones) seem to be important for FG and fecal pellets, with the difference that they were also important for SW samples.

Whereas in experiments 1 and 2 the 20 most differentially abundant predicted functions were more important in FG, FP2Hrs, FP24Hrs, and in some cases in SW samples, but with relatively low importance in EG samples, in experiment 3 an opposite pattern is observed. In fact, the top 20 predicted functions were always more important in EG and FP24Hrs samples, except for "Tryptophan 2,3-dioxygenase" (EC:1.13.11.11, rank 17), more important in EG and SW samples. Surprisingly, only a few predicted functions were consistently recovered among the 20 most differentially abundant predicted functions across experiments (e.g., EC:3.4.13.9, Xaa-Pro dipeptidase between experiments 1 and 2; EC:5.3.4.1, Protein disulfide-isomerase between experiments 1 and 3; Fig. 7).

The predicted functions/genes recovered in the *PICRUSt2* analysis, and differently abundant among sample types, were also grouped into key metabolic processes in the marine environment including nitrogen, carbon,

and sulfur cycling (Table S7, Appendix S1). The contribution of individual predicted functions/genes to the overall abundance was often low (i.e., RA < 0.1%) and varied according to the feeding experiment. Nevertheless, key genes such as those involved in the nitrogen (e.g., Ammonification: urease, Denitrification: narG, N reduction: nasA and nirB) and sulfur (e.g., Sulfate reduction: sat, met3) cycling were predicted to contribute to the functional potential found in the different sample types. Moreover, the major contributor (i.e., sample type) to a specific predicted function also varied according to the experiment. For example, the major contribution to narG (EC:1.7.99.4, Denitrification) came from SW, FG, and EG for experiments 1, 2, and 3, respectively. A complete list of the predicted functions/genes and their contribution to specific metabolic processes are given in Appendix S1 (Table S7).

4 DISCUSSION

4.1 Doliolid associated microbiome: patterns of abundance and diversity

This study investigated the associated microbiome of D. gegenbauri and how it may differed from their organic-rich fecal pellets and from the surrounding seawater, thus advancing our current knowledge on how pelagic tunicates such as doliolids may influence the microbial loop and key biogeochemical processes in the ocean (Frischer et al., 2021; Ishak et al., 2020; Koster & Paffenhofer, 2016). Amplicon 16S rRNA data from three independent feeding experiments suggested that the patterns of alpha and beta diversity among sample types were highly consistent. These patterns were also supported by complementary qPCR analysis, where FP24Hrs displayed a much higher bacterial abundance when compared to EG and SW samples. Bacterial communities associated with copepod fecal pellets were either more or less abundant than in the surrounding seawater (Delille & Razouls, 1994; Jing, Shek, Yung, Jin, & Liu, 2012) and might be attributed to different methodologies. For *D. gegenbauri*, Koster et al. (2014) reported much higher bacterial abundance in aged (i.e., four hrs or more) than fresh fecal pellets, and that food diet also played an important role. Studies focused on particle-associated marine microbes have shown quick colonization by bacterial taxa (40 hrs only) with clear successional patterns, and that these also differed from the free-living bacterial communities (Datta, Sliwerska, Gore, Polz, & Cordero, 2016; Roth Rosenberg et al., 2021; Yuan et al., 2021).

Differences observed across feeding experiments were most likely related to the different initial SW, which may represent the seasonal variability of the ocean microbiome (Shoemaker & Moisander, 2017; Yeh, Questel, Maas, & Bucklin, 2020) as well as individual-level differences among doliolids (Datta et al., 2018). Studies focused on the zooplankton microbiome, mostly crustaceans showed great differences between surrounding seawater and zooplankton-host species microbial communities, often more diverse in the former group (Datta et al., 2018; De Corte et al., 2018; Samad, Lee, Cerbin, Meima-Franke, & Bodelier, 2020; Shoemaker & Moisander, 2015). The highest values of alpha diversity were observed in SW samples followed closely by FP2Hrs/FP24Hrs and FG samples. Thus, it is expected that *D. gegenbauri* supports a more specialized microbiome that, at times, may significantly influence (directly or indirectly through their fecal pellets) the surrounding ocean microbiome and microbial-mediated processes (Frischer et al., 2021; Ishak et al., 2020; Koster & Paffenhofer, 2016; Turner, 2015).

In addition to low bacterial abundance as shown by the qPCR analysis, EG samples were always characterized by the lowest diversity. Association between greater bacterial biomass and the presence of food has been reported for copepods (Datta et al., 2018). Moreover, lack of food in the gut of copepod specimens entering a diapause stage and found in deeper depths was associated with distinct and less diverse microbial communities due to low nutrient availability (Datta et al., 2018). It is also possible that the physical-chemical conditions in the gut of D. gegenbauri and related gelatinous zooplankton hosts impose selective pressures on microbes as bacterial density in zooplankton hosts is much higher than that in the seawater, thus intensifying competition among bacteria (Datta et al., 2018; Samad et al., 2020).

High microbial diversity, as rich as that found in SW, was consistently observed in and fecal pellet samples across all experiments. Doliolids produce fecal pellets at high rates, and in conjunction with their high densities can have significant ecological impacts on the food web of pelagic systems (Ishak et al., 2020; Koster, Sietmann, Meuche, & Paffenhofer, 2011; Patonai et al., 2011; Turner, 2015). According to Koster

et al. (2011), doliolid fecal pellets can be colonized by bacteria in both external and internal surfaces, with abundances varying according to doliolid prey items. Once these fecal pellets are egested into the water column, they are rapidly colonized and degraded by the bacteria living in the surrounding seawater, thus increasing bacterial diversity in fecal pellets as observed herein and in the study of particle-associated marine microbes (Datta et al., 2016; Jing et al., 2012; Koster et al., 2011; Patonai et al., 2011; Roth Rosenberg et al., 2021; Turner, 2015; Yuan et al., 2021).

Microbial communities associated with fecal pellets and/or particle-aggregates have been well-characterized. Jing et al. (2012) showed that microbes associated with the copepod fecal pellets differed from that in the seawater (e.g., including unique taxa, *Sulfitobacter*). Although these differences decreased with the incubation period and degradation process, some bacterial taxa initially found in the fecal pellets were never recovered from seawater, suggesting these bacteria may reside in the copepod gut as part of their microbiome. Similarly, Cnudde et al. (2013) showed high internal microbial diversity in copepod fecal pellets, which was also strongly associated with the food source. However, their results were inconclusive with respect to the precise origin of gut bacteria (i.e., resident vs. transient). For particle-associated marine microbes, high-throughput sequencing studies have shown that these communities not only drastically differed from free-living bacterial fractions but also responded differently to environmental drivers and displayed differential metabolic potential (Datta et al., 2016; Roth Rosenberg et al., 2021; Yuan et al., 2021).

Zooplankton microbiome studies have shown differences between copepod and seawater microbes and between different copepod physiological stages (Datta et al., 2018); among suitable zooplankton-host species (De Corte et al., 2018); among native and non-indigenous gelatinous zooplankton species (Jaspers et al., 2020), and among bacterioplankton, zooplankton species, and particle-associated microbes (Samad et al., 2020). In this study, microbial communities were structured by sample type, a pattern consistent across all three experiments (Fig. 3). The great dissimilarity between EG and the other sample types is largely explained by the low alpha diversity and the low number of shared ASVs. Furthermore, low evenness in EG doliolids shows that their associated microbiome is dominated by only a few taxa (e.g., *Alteronomanas, Pelagibaca*; Fig. 2). Zooplankton species serve as nutrient-rich habitats for diverse bacteria that flourish as they feed in different food sources (Datta et al., 2018; De Corte et al., 2018). Thus, zooplankton feeding habits, including prey preferences, are key to supporting a diverse microbial community. For instance, the great majority of bacteria associated with doliolid fecal pellets occurred in the vicinity of partially digested food prey items such as diatoms which are known to harbor unique and temporally stable microbiomes (Behringer et al., 2018; Koster et al., 2011).

Full gut samples were more similar to F2Hrs with respect to their associated microbiome, which is not surprising since FG doliolids can produce fecal pellets in a matter of minutes. Their high similarity to FP24Hrs, however, brings additional evidence to the hypothesis that doliolids may reingest their fecal pellets as part of their feeding strategy (Koster & Paffenhofer, 2016; Koster et al., 2011). Previous studies showed that most of the material ingested by doliolids is not digested and/or assimilated and that they may reingest their fecal pellets in the absence and/or presence of phytoplankton in order to acquire additional nutrition (Frischer et al., 2021; Koster & Paffenhofer, 2016; Koster et al., 2011). Thus, the absorption of nutrients by doliolids may be facilitated by heterotrophic bacteria colonizing their fecal pellets. The relatively high similarity between SW and FP2Hrs/FP24Hrs samples also supports the idea that microbes available in the surrounding seawater can rapidly colonize the material secreted by doliolids (Frischer et al., 2021; Koster et al., 2011).

4.2 Major microbial taxa associated with doliolids

Microbial phyla associated with doliolids and other sample types were highly dominated by *Proteobacteria* (most notably *Alphaproteobacteria* and *Gammaproteobacteria*), regardless of the feeding experiment. Both *Proteobacteria* groups as well as *Cyanobacteria* and *Bacteroidota* are typical microbial taxa dominating the marine bacterioplankton community in diverse regions of the globe (Coutinho et al., 2021; da Silva & de Souza Lima, 2017; Schauer, Balague, Pedros-Alio, & Massana, 2003; Yilmaz et al., 2015). For the shallow waters of the South Atlantic Bight (SAB) where SW was collected, Lu et al. (2015) reported SAR11

(Alphaproteobacteria), Cyanobacteria(mostly Synechococcus ssp.), and to a lesser extent Rhodobacteraceae (Alphaproteobacteria) as the most abundant taxa in both spring and fall seasons.

SAR11 is adapted to grow in low nutrient concentrations and is commonly found in oligotrophic oceanic regions (Giovannoni, 2017; Morris et al., 2002). In this study, SAR11 was recovered in the SW samples of all three experiments and mostly represented by subgroups 1a, 1b, and 2, which are typically found in high abundance in shallow waters. Subgroups 3 and 4, extremely rare herein, are much less abundant in this pelagic zone, and often display stronger seasonal variability (Giovannoni, 2017; Vergin et al., 2013; Yilmaz et al., 2015). The role of SAR11 as part of the doliolid-associated microbiome seems to be insignificant as suggested by their absence/relatively low abundance in FG and EG samples. Their genome is very streamlined and as such, they lack the metabolic pathways to live on particle-aggregates (Dadon-Pilosof et al., 2017; Giovannoni, 2017; Giovannoni, Cameron Thrash, & Temperton, 2014).

Although doliolids ingest particles over a wide size range (Conley et al., 2018; Frischer et al., 2021; Walters et al., 2019), it is highly unlikely they actively exclude such small size bacteria during their feeding behavior. Changes in the cell surface properties of SAR11 (i.e., lower hydrophobicity) facilitate grazing avoidance from mucous filter feeders such as appendicularians (e.g., *Oikopleura albicans*), by conferring them a non-sticky cell surface (Dadon-Pilosof et al., 2017). Conversely, the nutrient-rich conditions in the doliolid gut may not be favorable for the growth of SAR11 (in part due to their reduced genome), especially in the presence of other bacteria (e.g., in FG samples) which may out-compete them (Giovannoni, 2017; Giovannoni et al., 2014; Norris, Levine, Fernandez, & Stocker, 2021). Lack or minimal SAR11 abundance in the gut diverse zooplankton taxa was previously reported, even when detected in the surrounding seawater (De Corte et al., 2018; Shoemaker & Moisander, 2015). The presence of SAR11 in the EG samples (Exp3: 5%), however, is explained by its potential for growing in nutrient-poor conditions in conjunction with a less diverse microbial community, which in turn minimizes competition in the doliolid gut (Datta et al., 2018; Giovannoni, 2017; Giovannoni et al., 2017; Giovannoni et al., 2014).

Overall, the microbial community composition of FG, FP2Hrs, and FP24Hrs samples was similar. *Rhodobacteraceae* and *Flavobacteraceae* were relatively abundant in these sample types in experiments 1. The former group lives in association with marine organisms and contributes to biofilm formation [e.g., colonizing the zooplankton exoskeleton; (Dang, Li, Chen, & Huang, 2008; De Corte et al., 2018; Yeh et al., 2020)]. *Flavobacteraceae*, on the other hand, is abundant in diatoms and other phytoplankton groups, which are preyed by doliolids (Frischer et al., 2021; Walters et al., 2019). Diatoms such as *Asterionellopsis glacialis* and *Nitzschia longissima* harbor unique microbiomes dominated by *Rhodobacteraceae* and with a fair contribution of *Flavobacteraceae* (Behringer et al., 2018). Similarly, Datta et al. (2018) suggested that *Flavobacteraceae* might reach high abundances in the copepod microbiome by "hitchhiking" into the gut through their feeding. Both*Rhodobacteraceae* and *Flavobacteraceae* are considered copiotrophic bacteria and able to rapidly grow in nutrient-rich conditions (Bolanos et al., 2021; Giovannoni, 2017; Giovannoni et al., 2014; Yilmaz et al., 2015) as it is expected in FG, FP2Hrs, and FP24Hrs samples.

In experiment 2, a drastic increase of the family Cyanobiaceae(Cyanobacteria), mostly represented by the genera Cyanobium and Synechococcus was observed for the same sample types (less so in FP2Hrs). A high abundance of Cyanobacteria in coastal waters has been associated with summer blooms and freshwater input (Kolda et al., 2020; Zamora-Terol, Novotny, & Winder, 2020). High Cyanobiaceaeabundance was reported by Zamora-Terol et al. (2020) in the gut of copepods and cladocerans during the summer season. Yeh et al. (2020) reported high Synechococcus abundance (> 50% of 16S rRNA reads) in the microbiome of the copepod Calanus finmarchicus from the Irminger Sea, North Atlantic, likely a result of its feeding habits. In the presence of other food sources, Synechococcus is avoided by C. finmarchicus , thus questioning whether this bacterium is a resident of the copepod microbiome (Yeh et al., 2020). Similarly, the acquisition of Synechococcus by D. gegenbauri is likely explained by its feeding habits as this bacterial taxon was only important in FG, FP2Hrs, and FP24Hrs samples, but tends to disappear in EG samples.

In experiment 3, multiple taxa belonging to the family Pirellulaceae (e.g., Blastopirellula, Pirellulaceae unknown genus, and Rubripirellula) and to a lesser extent Phycisphaerae, all part of the Plancto-

mycetota , were recovered in FG, FP2Hrs, and FP24Hrs. *Planctomycetota* abundance is usually low in epipelagic zones and is often associated with high productivity ocean waters (Coutinho et al., 2021; Yilmaz et al., 2015). The relative abundance of *Planctomycetota* in SW samples was very low across all feeding experiments but increased in FG, FP2Hrs, and FP24Hrs samples. Shoemaker and Moisander (2017) reported higher *Planctomycetota* abundance in the copepod gut than in seawater samples. *Planctomycetota* is known to perform well in anoxic conditions which are likely to be the case of the doliolid gut (De Corte et al., 2018; Tang, Glud, Glud, Rysgaard, & Nielsen, 2011; Yilmaz et al., 2015). This combination of low oxygen and high nutrients may aid*Planctomycetota* to thrive in the FG samples and consequently be recovered in the overall microbial community of starved *Centropages* copepods was very small (e.g., only *Pirellulaceae* being differently abundant), thus showing the importance of both factors in facilitating the growth of*Planctomycetota*.

Similarities for EG samples were also observed, especially the high contribution of *Enterobacterales* (Exp1: Alteromonas; Exp2/Exp3: Pseudoalteromonas). Moisander et al. (2015) reported both taxa as the most abundant microbes associated with different copepods species, especially in starved specimens. Furthermore, they showed that the association between starved *Centropages* and *Marinomonas*, which was also recovered in this study (Exp3: EG samples). On the other hand, De Corte et al. (2018) showed that *Flavobacteriales* and *Rhodobacterales* contributed greater to differentiate the copepod and seawater microbiomes, instead of *Enterobacterales*. The authors, however, did not distinguish between fed and starved copepods, potentially masking finer patterns (Moisander et al., 2015). The high contribution of either Alteromonas to differentiate the zooplankton and seawater microbiomes was also pointed out by other authors (Shoemaker et al., 2019; Shoemaker & Moisander, 2015).

When only considering EG samples, the complexity of the doliolid microbiome is relatively low, especially when compared to the other sample types. Low bacterial diversity has been reported for ctenophores (Daniels & Breitbart, 2012) and scyphozoans (Viver et al., 2017). Still, 29 AVSs were consistently recovered in EG samples across all three experiments; nine displayed a high frequency and may represent the doliolid "core" microbiome (e.g., *Alteromonas ,Pelagibaca*; Fig. 2).

4.3 Functional role of doliolids: implications for biogeochemical cycling

In this study, *PICRUSt2* (Douglas et al., 2020) was used to predict the functional potential of microbial communities associated with the different sample types, thus providing insights on how doliolids and their fecal pellets may impact the ocean microbial loop and metabolic processes involved. Although *PICRUSt2* may have its limitations in giving the "true picture" of the functional potential associated with microbial communities (Sun, Jones, & Fodor, 2020), the method has improved drastically in its most recent version with the implementation of more robust methods and a larger database for the comparison of query sequences (Douglas et al., 2020). Therefore, the results provided by *PICRUSt2* can certainly be used as a basis for generating hypotheses related to the functional potential of microbial communities associated with doliolids and their fecal pellets, which can be pursued in future research work by using more appropriate methods (Suarez-Moo et al., 2020; Voogd, de Voogd, Cleary, Polonia, & Gomes, 2015; Yilmaz et al., 2015).

The predicted functional analysis recovered in a larger number of functions/genes related to key metabolic processes. Those that contributed most (i.e., RA >0.1; Table S7, Appendix 1) to the functional potential of microbial communities associated with different sample types are discussed here. For example, key genes involved in the nitrogen cycling including *nasA* and *nirB*(i.e., involved in N reduction) were predicted in all three experiments with greater contributions from SW in experiment 1, FG experiment 2, and EG in experiment 3. These and other important genes (e.g., *nifH*, *nirS*, *nirK*, *nosZ*) involved in denitrification processes (De Corte et al., 2018; Espenberg et al., 2018) were also detected in the predicted functional analysis. Scavotto et al. (2015), studying the association of nitrogen-fixing bacteria and copepods, reported *nifH* in seawater particles and full gut copepods which led the authors to conclude that copepods may acquire *nifH* through feeding. In this study, major contributions to the predicted *nifH* gene also came from FG and EG doliolids. On the other hand, the contribution from SW samples was relatively low which suggests that

doliolids may acquire *nifH* differently than copepods.

Predicted functions to degrade organic compounds such as chitin (EC:3.2.1.14, Chitinase) were also detected in the analysis, especially in FP24Hrs (Exp1) and EG (Exp2 and Exp3) samples. Similarly, De Corte et al. (2018), using a metagenomic approach, showed the potential of zooplankton-associated bacterial communities in metabolizing *chitin* and other complex molecules. Scavotto et al. (2015) associated *chitin* degradation with bacterial communities dominated by *Vibrio* spp., which seems not to be the case for doliolids once the contribution of this genus to FG and EG samples was extremely low. Conversely, chitinases have been also found in *Pseudoalteronomas* ssp. (Cottrell, Wood, Yu, & Kirchman, 2000), a taxon extremely abundant in EG samples of experiment 2. In fact, the predicted abundance of *chitin* in the present was also highest in EG samples of experiment 2.

Unfortunately, only a few studies have characterized the microbial communities associated with gelatinous zooplankton hosts [e.g., ctenophores, scyphomedusae; (Hao et al., 2019; Hao, Gerdts, Peplies, & Wichels, 2015). These investigations, however, were restricted to community structure and diversity analysis and did not include information with respect to the potential metabolic capability. In this sense, our comparisons with respect to the functional role of doliolids were mostly restricted to copepods. Nevertheless, our results suggest that some of the predicted functions reported for doliolids are also shared by crustacean zooplankton hosts.

5 CONCLUSIONS

To our knowledge, this is the first study aiming to characterize the bacterial communities associated with doliolids and their fecal pellets using a metabarcoding approach. Overall, our results suggest that these microbial communities may play important roles in the biology and ecology of this important gelatinous zooplankton as well as on key metabolic processes taking place on the surrounding seawater. While many factors (e.g., food source, inter-individual variability) may influence the composition and stability of the doliolid-associated microbiome, our analysis focused solely on EG samples suggest that some microbial taxa are likely to be part of a resident microbiome. Furthermore, our 16S rRNA metabarcoding clearly distinguished the bacterial communities associated with the different sample types, which were also related to strong differences in microbial diversity and composition. Although limited, our predicted functional analysis with *PICRUst2* provides novel insights regarding the potential metabolic capability of *D. gegenbauri*-associated bacteria. Further work, using metagenomic approaches, is needed to elucidate the functional roles of microorganisms associated with doliolids. Future studies should also examine the microbiome associated with the different feeding preferences (Frischer et al., 2021), and assess the factors driving the temporal variability in doliolid-associated bacterial communities and how it may relate to changes in the ocean bacterioplankton.

AUTHOR CONTRIBUTIONS

T.J.P., T.L.W., H.M.B., and M.E.F. designed and conceived the study, contributed to data analysis, and wrote the manuscript. T.J.P. completed 16S rRNA PCR amplification, prepared libraries for Illumina sequencing, processed raw sequence data analysis, and executed bioinformatics workflows. T.L.W. performed feeding experiments and performed DNA extractions from all sample types. H.M. E. conducted qPCR analysis and provided intellectual contributions to the manuscript. All authors read and approved the final version of the manuscript.

ACKNOWLEDGEMENTS

This study was supported in part by the U.S. National Science Foundation collaborative awards OCE 1459293 and OCE 2023133 (M.E.F) and institutional startup funding from the University of Georgia (H.M.B). We would like to thank the hardworking and professional crew of the R/V Savannah for collecting seawater samples that were used in this study.

DATA AVAILABILITY STATEMENT

Raw Illumina reads generated in this study have been submitted to the NCBI Sequence Read Archive (BioProject XXXXXXXX and SRA accession XXXXXXXXX). Primer constructs, QIIME mapping files, and final ASV tables have been deposited in FigShare (*https://doi.org/10.6084/m9.figshare.5701090*). All scripts used for processing and analyzing the data are available on GitHub (*https://github.com/BikLab/doliolids*).

Tables

Table 1 . Summary (mean values) of different metrics (i.e., number of reads and alpha-diversity indices) for sample types according to each experiment. In each experiment, the lowest (light orange) and highest (light blue) values for each metric are highlighted. Kruskal-Wallis analysis was used to test for significant differences (p<0.05) among sample types. Pairwise comparisons among sample types with adjusted p-values (BH method) are given in Table S2.

Figure Legends

Figure 1. Univariate descriptors (mean +-SE) for microbial communities associated with doliolids (FG and EG), fecal pellets (FP2Hrs and FP24Hrs), and seawater (SW) samples in different feeding experiments (1-3). Observed diversity refers to the number of ASVs (i.e., unique sequences). For significant differences (p<0.05) in pairwise comparisons among sample types, the reader is referred to Table S2.

Figure 2. Abundance (mean +-SE) of nine frequently recovered bacterial taxa (i.e., [?] 50%) in EG samples across different feeding experiments. Abundance values are presented on a logarithmic scale. Additional information, including from other taxa often recovered in EG samples, is provided in Table S3.

Figure 3. Microbial community structure according to experiment (A: experiment 1, B: experiment 2, C: experiment 3) and sample types: doliolids (FG and EG), fecal pellets (FP2Hrs and FP24Hrs), and seawater (SW) in different feeding experiments (1-3). The nMDS ordination is based on the Bray-Curtis similarity constructed from the relative abundance of AVSs (square root transformed). Control samples and AVSs determined to be contaminants were removed from the analysis (see Methods for additional details).

Figure 4. Microbial community composition associated with doliolids (FG and EG), fecal pellets (FP2Hrs and FP24Hrs), and seawater (SW) samples in different feeding experiments (1-3). Taxonomy of the 11 most abundant bacterial phyla (A) and orders (B) are given. Low abundance taxa were grouped into the "Others" category. Relative abundance of taxa contributing to [?]5% is displayed in the barplots.

Figure 5. Microbial community composition associated with doliolids (FG and EG), fecal pellets (FP2Hrs and FP24Hrs), and seawater (SW) samples in different feeding experiments (1-3). Taxonomy of the 19 most abundant bacterial families (A) and genera (B) are given. Low abundance taxa were grouped into the "Others" category. Relative abundance of taxa contributing to [?]5% is displayed in the barplots.

Figure 6. Heatmap of the 10 most differentially abundant microbial taxa (phylum and genus level) across sample types (EG: empty gut, FG: full gut, FP24Hrs: fecal pellet 24Hrs, FP2Hrs: fecal pellet 2Hrs, SW: seawater) and experiments (A: Experiment 1, B: Experiment 2, C: Experiment 3). Taxon abundance was transformed using the centered-log ratio (CLR). For each taxon, warm colors indicate high abundance whereas cold colors indicate low abundance. A complete list of taxa differentially abundant for each taxonomic rank across sample types is provided in Table S5.

Figure 7. Heatmap of the 20 most differentially abundant predicted functional genes across sample types (EG: empty gut, FG: full gut, FP24Hrs: fecal pellet 24Hrs, FP2Hrs: fecal pellet 2Hrs, SW: seawater) and experiments (A: Experiment 1, B: Experiment 2, C: Experiment 3). The abundance of different functions/genes was transformed using the centered-log ratio (CLR). Warm colors indicate high abundance whereas cold colors indicate low abundance. A complete list of functions/genes differentially abundant, including their description, for each experiment and across sample types is provided in Table S6.

Supporting/Supplemental Information

Appendix S1

Table S1. Sequencing depth, including descriptive metrics (i.e., mean, median, SD) across sample types and three experiments. Data include the number of reads (i.e., input) fed to and retained (non-chimeric) by DADA2 as well as the number of unique DNA sequences (i.e., ASVs). The final read and ASV counts (i.e., after decontam) of each experimental dataset was used for statistical and ecological analyses.

Table S2 . Pairwise comparisons for the number of reads and alpha diversity metrics across sample types in each experiment. Bold values indicate significant differences (p <0.05) after correction for FD using the BH method.

Table S3. Bacterial taxa shared by 29 EG samples from all three feeding experiments. Highly frequent taxa (i.e., [?] 50%) are highlighted in green. For each bacterial taxon, mean abundance values (including Min-Max) and frequency are provided.

Table S4. Summary results from PERMANOVA analysis including pairwise comparisons among sample types for each experiment. Average similarity within (diagonal values in bold) and among sample types are also provided. Abbreviations: df: degrees of freedom; SS: sum of squares; MS: mean square; Pseudo-F: F statistic; P(MC): p-value obtained with Monte Carlo permutation test; Res: residual.

Table S5. Results from differential abundant analysis with *ALDEx2* for microbial taxa (phylum to genus level) across sample types (EG: empty gut, FG: full gut, FP24Hrs: fecal pellet 24Hrs, FP2Hrs: fecal pellet 2Hrs, SW: seawater) and experiments (Experiment 1, Experiment 2, Experiment 3). Taxon total abundance (and relative abundance RA%) is given for each sample type.

Table S6. Results from differential abundant analysis with ALDEx2 for predicted functional functions across sample types (EG: empty gut, FG: full gut, FP24Hrs: fecal pellet 24Hrs, FP2Hrs: fecal pellet 2Hrs, SW: seawater) and experiments (Experiment 1, Experiment 2, Experiment 3). Total abundance (and relative abundance RA%) of predicted functions across sample types is provided.

Table S7. *PICRUSt2* prediction results for the different sample types (FG, EG, FP2Hrs, FP24Hrs, and SW) and feeding experiments. Predicted function abundances are provided (i.e., per sample type, total, and overall relative abundance – RA%). For each experiment, predicted functions were grouped into energy, carbon, nitrogen, sulfur, phosphate, and other metabolisms.

Appendix S2

Figure S1. Microbial community structure of the unfiltered dataset. All three experiments are included in the same analysis. Sample types: doliolids (FG and EG), fecal pellets (FP2Hrs and FP24Hrs), seawater (SW), and controls (i.e., positive and negative). The nMDS ordination is based on the Bray-Curtis similarity constructed from the relative abundance of AVSs (square root transformed).

Figure S2. Abundance (mean +-SE) of bacterial communities associated with EG, FP24Hrs, and SW samples. Bacterial abundance was inferred from 16S rRNA gene copy abundance quantified by quantitative PCR (qPCR) and normalized to sample volume.

Figure S3. Venn diagram showing the number of unique (highlighted in bold) and shared AVSs among sample types for (A) experiment 1, (B) experiment 2, and (C) experiment 3. Doliolids: FG and EG, fecal pellets: FP2Hrs and FP24Hrs, seawater: SW.

Figure S4. Venn diagram showing the number of unique (highlighted in bold) and shared AVSs among experiments. (A) Empty Gut, (B) Full Gut, (C) Fecal Pellets 2Hrs, (D) Fecal Pellets 24Hrs, and (E) Seawater.

Figure S5. Relative abundance of four dominant phyla associated with doliolids (FG and EG), fecal pellets (FP2Hrs and FP24Hrs), and seawater (SW) samples in different feeding experiments (1-3). Low abundance phyla (< 10%) are represented by the "Others" category. Relative abundance of taxa contributing to [?]5%

is displayed in the barplots. Phyla abbreviations as follows: *Bacteroidota*(Bact.), *Cyanobacteria* (Cyanob.), *Planctomycetota*(Planct.), *Proteobacteria* (Proteo.).

REFERENCES

Allen, A. E., Booth, M. G., Verity, P. G., & Frischer, M. E. (2005). Influence of nitrate availability on the distribution and abundance of heterotrophic bacterial nitrate assimilation genes in the Barents Sea during summer. *Aquatic microbial ecology*, 39 (3), 247-255. doi:10.3354/ame039247

Alldredge, A. L., & Madin, L. P. (1982). Pelagic tunicates: unique herbivores in the marine plankton. *Bioscience*, 32(8), 655–663. doi: 10.2307/1308815

Anderson, M., Gorley, R., & Clarke, K. P. (2008). *PERMANOVA for PRIMER: guide to software and statistical methods*. PRIMER-e.

Apprill, A., McNally, S., Parsons, R., & Weber, L. (2015). Minor revision to V4 region SSU rRNA 806R gene primer greatly increases detection of SAR11 bacterioplankton. *Aquatic Microbial Ecology: International Journal*, 75(2), 129–137. doi: 10.3354/ame01753

Behringer, G., Ochsenkuhn, M. A., Fei, C., Fanning, J., Koester, J. A., & Amin, S. A. (2018). Bacterial communities of diatoms display strong conservation across strains and time. *Frontiers in Microbiology*, 9, 659. doi: 10.3389/fmicb.2018.00659

Benjamini, Y., & Hochberg, Y. (1995). Controlling the false discovery rate: a practical and powerful approach to multiple testing. *Journal of the Royal Statistical Society: Series B (Methodological)*, 57(1), 289–300. doi: 10.1111/j.2517-6161.1995.tb02031.x

Boero, F., Bouillon, J., Gravili, C., Miglietta, M. P., Parsons, T., & Piraino, S. (2008). Gelatinous plankton: irregularities rule the world (sometimes). *Marine Ecology Progress Series*, 356, 299–310. doi: 10.3354/meps07368

Bolanos, L. M., Choi, C. J., Worden, A. Z., Baetge, N., Carlson, C. A., & Giovannoni, S. (2021). Seasonality of the microbial community composition in the North Atlantic. *Frontiers in Marine Science*, 8. doi: 10.3389/fmars.2021.624164

Bolyen, E., Rideout, J. R., Dillon, M. R., Bokulich, N. A., Abnet, C. C., Al-Ghalith, G. A., ... Caporaso, J. G. (2019). Reproducible, interactive, scalable and extensible microbiome data science using QIIME 2. *Nature Biotechnology*, *37*(8), 852–857. doi: 10.1038/s41587-019-0209-9

Bone, Q. (1998). The biology of pelagic tunicates (Q. Bone, ed.). London, England: Oxford University Press.

Callahan, B. J., McMurdie, P. J., Rosen, M. J., Han, A. W., Johnson, A. J. A., & Holmes, S. P. (2016). DADA2: High-resolution sample inference from Illumina amplicon data. *Nature Methods*, 13(7), 581–583. doi: 10.1038/nmeth.3869

Camacho, C., Coulouris, G., Avagyan, V., Ma, N., Papadopoulos, J., Bealer, K., & Madden, T. L. (2009). BLAST : architecture and applications. *BMC Bioinformatics*, 10(1), 421. doi: 10.1186/1471-2105-10-421

Caporaso, J. G., Lauber, C. L., Walters, W. A., Berg-Lyons, D., Huntley, J., Fierer, N., ... Knight, R. (2012). Ultra-high-throughput microbial community analysis on the Illumina HiSeq and MiSeq platforms. *The ISME Journal*, 6(8), 1621–1624. doi: 10.1038/ismej.2012.8

Clarke, K. R. (1993). Non-parametric multivariate analyses of changes in community structure. *Australian Journal of Ecology*, 18(1), 117–143. doi/abs/10.1111/j.1442-9993

Cnudde, C., Sanchez Clavano, C. J., Moens, T., Willems, A., & De Troch, M. (2013). Structural and functional patterns of active bacterial communities during aging of harpacticoid copepod fecal pellets. *Aquatic Microbial Ecology: International Journal*, 71(1), 25–42. doi: 10.3354/ame01663 Condon, R. H., Steinberg, D. K., del Giorgio, P. A., Bouvier, T. C., Bronk, D. A., Graham, W. M., & Ducklow, H. W. (2011). Jellyfish blooms result in a major microbial respiratory sink of carbon in marine systems. *Proceedings of the National Academy of Sciences of the United States of America*, 108(25), 10225–10230. doi: 10.1073/pnas.1015782108

Conley, K. R., Lombard, F., & Sutherland, K. R. (2018). Mammoth grazers on the ocean's minuteness: a review of selective feeding using mucous meshes. *Proceedings. Biological Sciences / The Royal Society*, 285(1878). doi: 10.1098/rspb.2018.0056

Cottrell, M. T., Wood, D. N., Yu, L., & Kirchman, D. L. (2000). Selected chitinase genes in cultured and uncultured marine bacteria in the alpha- and gamma-subclasses of the proteobacteria. *Applied and Environmental Microbiology*, 66(3), 1195–1201. doi: 10.1128/AEM.66.3.1195-1201.2000

Coutinho, F. H., von Meijenfeldt, F. A. B., Walter, J. M., Haro-Moreno, J. M., Lopez-Perez, M., van Verk, M. C., ... Thompson, F. L. (2021). Ecogenomics and metabolic potential of the South Atlantic Ocean microbiome. *The Science of the Total Environment*, 765, 142758. doi: 10.1016/j.scitotenv.2020.142758

Crocker, K. M., Alldredge, A. L., & Steinberg, D. K. (1991). Feeding rates of the doliolid, *Dolioletta gegen*bauri, on diatoms and bacteria. *Journal of Plankton Research*, 13(1), 77–82. doi: 10.1093/plankt/13.1.77

Dadon-Pilosof, A., Conley, K. R., Jacobi, Y., Haber, M., Lombard, F., Sutherland, K. R., ... Yahel, G. (2017). Surface properties of SAR11 bacteria facilitate grazing avoidance. *Nature Microbiology*, 2(12), 1608–1615. doi: 10.1038/s41564-017-0030-5

Dang, H., Li, T., Chen, M., & Huang, G. (2008). Cross-ocean distribution of *Rhodobacterales* bacteria as primary surface colonizers in temperate coastal marine waters. *Applied and Environmental Microbiology*, 74(1), 52–60. doi: 10.1128/AEM.01400-07

Daniels, C., & Breitbart, M. (2012). Bacterial communities associated with the ctenophores *Mnemiopsis* leidyi and Beroe ovata. FEMS Microbiology Ecology, 82(1), 90–101. doi: 10.1111/j.1574-6941.2012.01409.x

da Silva, M. A. C., & de Souza Lima, A. O. (2017). Diversity and prospection of South Atlantic Ocean microorganisms. In J. L. de Azevedo & M. C. Quecine (Eds.), *Diversity and benefits of microorganisms from the tropics* (pp. 105–136). Springer International Publishing. doi: 10.1007/978-3-319-55804-2_6

Datta, M. S., Almada, A. A., Baumgartner, M. F., Mincer, T. J., Tarrant, A. M., & Polz, M. F. (2018). Inter-individual variability in copepod microbiomes reveals bacterial networks linked to host physiology. *The ISME Journal*, 12(9), 2103–2113. doi: 10.1038/s41396-018-0182-1

Datta, M. S., Sliwerska, E., Gore, J., Polz, M. F., & Cordero, O. X. (2016). Microbial interactions lead to rapid micro-scale successions on model marine particles. *Nature Communications*, 7(1). doi: 10.1038/ncomms11965

Davis, N. M., Proctor, D. M., Holmes, S. P., Relman, D. A., & Callahan, B. J. (2018). Simple statistical identification and removal of contaminant sequences in marker-gene and metagenomics data. *Microbiome*, 6(1), 226. doi: 10.1186/s40168-018-0605-2

De Corte, D., Srivastava, A., Koski, M., Garcia, J. A. L., Takaki, Y., Yokokawa, T., ... Herndl, G. J. (2018). Metagenomic insights into zooplankton-associated bacterial communities. *Environmental Microbiology*, 20(2), 492–505. doi: 10.1111/1462-2920.13944

Deibel, D. (1985). Blooms of the pelagic tunicate, *Dolioletta gegenbauri*: Are they associated with Gulf Stream frontal eddies? *Journal of Marine Research*, 43(1), 211–236. doi: 10.1357/002224085788437307

Deibel, D. (1990). Still-water sinking velocity of fecal material from the pelagic tunicate *Dolioletta gegenbauri*. Marine Ecology Progress Series, 62(1), 55–60.

Deibel, D., & Paffenhofer, G.-A. (1988). Cinematographic analysis of the feeding mechanism of the pelagic tunicate *Doliolum Nationalis*. *Bulletin of Marine Science*, 43(3), 404–412.

Deibel, D., & Paffenhofer, G.-A. (2009). Predictability of patches of neritic salps and dollolids (Tunicata, Thaliacea). Journal of Plankton Research, 31 (12), 1571–1579. doi: 10.1093/plankt/fbp091

Delille, D., & Razouls, S. (1994). Community structures of heterotrophic bacteria of copepod fecal pellets. *Journal of Plankton Research*, 16(6), 603–615. doi: 10.1093/plankt/16.6.603

Douglas, G. M., Maffei, V. J., Zaneveld, J. R., Yurgel, S. N., Brown, J. R., Taylor, C. M., ... Langille, M. G. I. (2020). PICRUSt2 for prediction of metagenome functions. *Nature Biotechnology*, 38(6), 685–688. doi: 10.1038/s41587-020-0548-6

Eckert, E. M., Anicic, N., & Fontaneto, D. (2021). Freshwater zooplankton microbiome composition is highly flexible and strongly influenced by the environment. *Molecular Ecology*, 30(6), 1545–1558. doi: 10.1111/mec.15815

Espenberg, M., Truu, M., Mander, U., Kasak, K., Nolvak, H., Ligi, T., ... Truu, J. (2018). Differences in microbial community structure and nitrogen cycling in natural and drained tropical peatland soils. *Scientific Reports*, 8(1), 4742. doi: 10.1038/s41598-018-23032-y

Fernandes, A. D., Macklaim, J. M., Linn, T. G., Reid, G., & Gloor, G. B. (2013). ANOVA-like differential expression (ALDEx) analysis for mixed population RNA-Seq.*PloS One*, 8(7), e67019. doi: 10.1371/journal.pone.0067019

Fernandes, A. D., Reid, J. N., Macklaim, J. M., McMurrough, T. A., Edgell, D. R., & Gloor, G. B. (2014). Unifying the analysis of high-throughput sequencing datasets: characterizing RNA-seq, 16S rRNA gene sequencing and selective growth experiments by compositional data analysis. *Microbiome*, 2, 15. doi: 10.1186/2049-2618-2-15

Frischer, M. E., Lamboley, L. M., Walters, T. L., Brandes, J. A., Arneson, E., Lacy, L. E., ... Gibson, D. M. (2021). Selective feeding and linkages to the microbial food web by the doliolid *Dolioletta gegenbauri*. *Limnology and Oceanography*, 66(5), 1993–2010. doi: 10.1002/lno.11740

Gibson, D. M. (2000). Feeding and growth rates of the doliolid, *Dolioletta gegenbauri* Uljanin (Tunicata, Thaliacea). *Journal of Plankton Research*, 22(8), 1485–1500. doi: 10.1093/plankt/22.8.1485

Giovannoni, S. J. (2017). SAR11 Bacteria: The most abundant plankton in the oceans. Annual Review of Marine Science, 9, 231–255. doi: 10.1146/annurev-marine-010814-015934

Giovannoni, S. J., Cameron Thrash, J., & Temperton, B. (2014). Implications of streamlining theory for microbial ecology. *The ISME Journal*, 8(8), 1553–1565. doi: 10.1038/ismej.2014.60

Greer, A. T., Boyette, A. D., Cruz, V. J., Cambazoglu, M. K., Dzwonkowski, B., Chiaverano, L. M., ... Wiggert, J. D. (2020). Contrasting fine-scale distributional patterns of zooplankton driven by the formation of a diatom-dominated thin layer. *Limnology and Oceanography*, 65(9), 2236–2258. doi: 10.1002/lno.11450

Greer, A. T., Chiaverano, L. M., Treible, L. M., Briseno-Avena, C., & Hernandez, F. J. (2021). From spatial pattern to ecological process through imaging zooplankton interactions. *ICES Journal of Marine Science: Journal Du Conseil*, 78(8), 2664–2674. doi: 10.1093/icesjms/fsab149

Hao, W., Gerdts, G., Holst, S., & Wichels, A. (2019). Bacterial communities associated with scyphomedusae at Helgoland Roads. *Marine Biodiversity*, 49(3), 1489–1503. doi: 10.1007/s12526-018-0923-4

Hao, W., Gerdts, G., Peplies, J., & Wichels, A. (2015). Bacterial communities associated with four ctenophore genera from the German Bight (North Sea). *FEMS Microbiology Ecology*, 91(1), 1–11. doi: 10.1093/femsec/fiu006

Ishak, N. H. A., Tadokoro, K., Okazaki, Y., Kakehi, S., Suyama, S., & Takahashi, K. (2020). Distribution, biomass, and species composition of salps and doliolids in the Oyashio–Kuroshio transitional region: potential impact of massive bloom on the pelagic food web. *Journal of Oceanography*, 76(5), 351–363. doi: 10.1007/s10872-020-00549-3 Jaspers, C., Weiland-Brauer, N., Ruhlemann, M. C., Baines, J. F., Schmitz, R. A., & Reusch, T. B. H. (2020). Differences in the microbiota of native and non-indigenous gelatinous zooplankton organisms in a low saline environment. *The Science of the Total Environment*, 734, 139471. doi: 10.1016/j.scitotenv.2020.139471

Jing, H., Shek, L., Yung, W., Jin, X., & Liu, H. (2012). Dynamics of bacterial community composition during degradation of copepod fecal pellets. *Journal of Plankton Research*, 34(8), 700–710. doi: 10.1093/plankt/fbs043

Kolda, A., Ljubešić, Z., Gavrilović, A., Jug-Dujaković, J., Pikelj, K., & Kapetanović, D. (2020). Metabarcoding Cyanobacteria in coastal waters and sediment in central and southern Adriatic Sea. *Acta Botanica Croatica*, 79(2), 157–169. doi: 10.37427/botcro-2020-021

Köster, M., & Paffenhöfer, G.-A. (2016). How efficiently can doliolids (Tunicata, Thaliacea) utilize phytoplankton and their own fecal pellets? *Journal of Plankton Research*. doi: 10.1093/plankt/fbw089

Köster, M., Paffenhöfer, G.-A., Schlüter, R., & Meuche, A. (2014). Time-series observations of prokaryotic colonization of zooplankton fecal pellets. *Journal of Plankton Research*, 36(6), 1461–1475. doi: 10.1093/plankt/fbu060

Köster, M., Sietmann, R., Meuche, A., & Paffenhöfer, G.-A. (2011). The ultrastructure of a doliolid and a copepod fecal pellet. *Journal of Plankton Research*, 33(10), 1538–1549. doi: 10.1093/plankt/fbr053

Lebrato, M., Pahlow, M., Frost, J. R., & Küter, M. (2019). Sinking of gelatinous zooplankton biomass increases deep carbon transfer efficiency globally. *Global*. Retrieved from https://agupubs.onlinelibrary.wiley.com/doi/abs/10.1029/2019GB006265

Lucas, C. H., & Dawson, M. N. (2014). What are jellyfishes and thaliaceans and why do they bloom? In K. A. Pitt & C. H. Lucas (Eds.), *Jellyfish Blooms* (pp. 9–44). Dordrecht: Springer Netherlands. doi: 10.1007/978-94-007-7015-7_2

Lu, X., Sun, S., Zhang, Y.-Q., Hollibaugh, J. T., & Mou, X. (2015). Temporal and vertical distributions of bacterioplankton at the Gray's Reef National Marine Sanctuary. *Applied and Environmental Microbiology*, 81(3), 910–917. doi: 10.1128/AEM.02802-14

Martin, B., Koppelmann, R., & Kassatov, P. (2016). Ecological relevance of salps and doliolids in the northern Benguela Upwelling System. *Journal of Plankton Research*, 39(2), 290–304. doi: 10.1093/plankt/fbw095

Martin, M. (2011). Cutadapt removes adapter sequences from high-throughput sequencing reads. *EMBnet.journal*, 17(1), 10. doi: 10.14806/ej.17.1.200

McMurdie, P. J., & Holmes, S. (2013). phyloseq: an R package for reproducible interactive analysis and graphics of microbiome census data. *PloS One*, 8(4), e61217. doi: 10.1371/journal.pone.0061217

Moisander, P. H., Sexton, A. D., & Daley, M. C. (2015). Stable associations masked by temporal variability in the marine copepod microbiome. *PloS One*, 10(9), e0138967. doi: 10.1371/journal.pone.0138967

Morris, R. M., Rappé, M. S., Connon, S. A., Vergin, K. L., Siebold, W. A., Carlson, C. A., & Giovannoni, S. J. (2002). SAR11 clade dominates ocean surface bacterioplankton communities. *Nature*, 420(6917), 806–810. doi: 10.1038/nature01240

Norris, N., Levine, N. M., Fernandez, V. I., & Stocker, R. (2021). Mechanistic model of nutrient uptake explains dichotomy between marine oligotrophic and copiotrophic bacteria. *PLoS Computational Biology*, 17(5), e1009023. doi: 10.1371/journal.pcbi.1009023

Parada, A. E., Needham, D. M., & Fuhrman, J. A. (2016). Every base matters: assessing small subunit rRNA primers for marine microbiomes with mock communities, time series and global field samples. *Environmental Microbiology*, 18(5), 1403–1414. doi: 10.1111/1462-2920.13023

Patonai, K., El-Shaffey, H., & Paffenhöfer, G.-A. (2011). Sinking velocities of fecal pellets of doliolids and calanoid copepods. *Journal of Plankton Research*, 33(7), 1146–1150. doi: 10.1093/plankt/fbr011

Quast, C., Pruesse, E., Yilmaz, P., Gerken, J., Schweer, T., Yarza, P., ... Glöckner, F. O. (2013). The SILVA ribosomal RNA gene database project: improved data processing and web-based tools. *Nucleic Acids Research*, 41 (Database issue), D590–D596. doi: 10.1093/nar/gks1219

R Core Team. (2021). R: A language and environment for statistical computing (Version 4.1.2). R Foundation for Statistical Computing, Vienna, Austria. Retrieved from https://www.R-project.org

Richardson, T. L. (2019). Mechanisms and pathways of small-phytoplankton export from the surface ocean. Annual Review of Marine Science, 11, 57–74. doi: 10.1146/annurev-marine-121916-063627

Roth Rosenberg, D., Haber, M., Goldford, J., Lalzar, M., Aharonovich, D., Al-Ashhab, A., ... Sher, D. (2021). Particle-associated and free-living bacterial communities in an oligotrophic sea are affected by different environmental factors. *Environmental Microbiology*, 23(8), 4295–4308. doi: 10.1111/1462-2920.15611

Samad, M. S., Lee, H. J., Cerbin, S., Meima-Franke, M., & Bodelier, P. L. E. (2020). Niche differentiation of host-associated pelagic microbes and their potential contribution to biogeochemical cycling in artificially warmed lakes. *Frontiers in Microbiology*, 11, 582. doi: 10.3389/fmicb.2020.00582

Scavotto, R. E., Dziallas, C., Bentzon-Tilia, M., Riemann, L., & Moisander, P. H. (2015). Nitrogen-fixing bacteria associated with copepods in coastal waters of the North Atlantic Ocean. *Environmental Microbiology*, 17(10), 3754–3765. doi: 10.1111/1462-2920.12777

Schauer, M., Balagué, V., Pedrós-Alió, C., & Massana, R. (2003). Seasonal changes in the taxonomic composition of bacterioplankton in a coastal oligotrophic system. *Aquatic Microbial Ecology: International Journal*, *31*, 163–174. doi: 10.3354/ame031163

Schuelke, T., Pereira, T. J., Hardy, S. M., & Bik, H. M. (2018). Nematode-associated microbial taxa do not correlate with host phylogeny, geographic region or feeding morphology in marine sediment habitats. *Molecular Ecology*, 27(8), 1930–1951. doi: 10.1111/mec.14539

Shoemaker, K. M., Duhamel, S., & Moisander, P. H. (2019). Copepods promote bacterial community changes in surrounding seawater through farming and nutrient enrichment. *Environmental Microbiology*, 21 (10), 3737–3750. doi: 10.1111/1462-2920.14723

Shoemaker, K. M., & Moisander, P. H. (2015). Microbial diversity associated with copepods in the North Atlantic subtropical gyre. *FEMS Microbiology Ecology*, 91(7). doi: 10.1093/femsec/fiv064

Shoemaker, K. M., & Moisander, P. H. (2017). Seasonal variation in the copepod gut microbiome in the subtropical North Atlantic Ocean. *Environmental Microbiology*, 19(8), 3087–3097. doi: 10.1111/1462-2920.13780

Suárez-Moo, P., Cruz-Rosales, M., Ibarra-Laclette, E., Desgarennes, D., Huerta, C., & Lamelas, A. (2020). Diversity and composition of the gut microbiota in the developmental stages of the dung beetle *Copris* incertus Say (Coleoptera, Scarabaeidae). Frontiers in Microbiology, 11. doi: 10.3389/fmicb.2020.01698

Sullivan, L. J., & Kremer, P. (2011). Gelatinous zooplankton and their trophic roles. In E. Wolanski & D. McLusky (Eds.), *Trophic relationships of coastal and estuarine ecosystems* (Vol. 6, pp. 127–171). Elsevier.

Sun, S., Jones, R. B., & Fodor, A. A. (2020). Inference-based accuracy of metagenome prediction tools varies across sample types and functional categories. *Microbiome*, 8(1), 46. doi: 10.1186/s40168-020-00815-y

Takahashi, K., Ichikawa, T., Fukugama, C., Yamane, M., Kakehi, S., Okazaki, Y., ... Furuya, K. (2015). In situ observations of a doliolid bloom in a warm water filament using a video plankton recorder: Bloom development, fate, and effect on biogeochemical cycles and planktonic food webs. *Limnology and Oceanography*, 60(5), 1763–1780. doi: 10.1002/lno.10133

Tang, K. W., Backhaus, L., Riemann, L., Koski, M., Grossart, H.-P., Munk, P., & Nielsen, T. G. (2019). Copepod carcasses in the subtropical convergence zone of the Sargasso Sea: implications for microbial community composition, system respiration and carbon flux. *Journal of Plankton Research*,41(4), 549–560. doi: 10.1093/plankt/fbz038

Tang, K. W., Glud, R. N., Glud, A., Rysgaard, S., & Nielsen, T. G. (2011). Copepod guts as biogeochemical hotspots in the sea: Evidence from microelectrode profiling of *Calanus* spp. *Limnology and Oceanogra-phy*, 56(2), 666–672. doi: 10.4319/lo.2011.56.2.0666

Tebeau, C. M., & Madin, L. P. (1994). Grazing rates for three life history stages of the doliolid*Dolioletta gegenbauri* Uljanin (Tunicata, Thaliacea). *Journal of Plankton Research*, 16(8), 1075–1081. doi: 10.1093/plankt/16.8.1075

Thompson, L. R., Sanders, J. G., McDonald, D., Amir, A., Ladau, J., Locey, K. J., ... Earth Microbiome Project Consortium. (2017). A communal catalogue reveals Earth's multiscale microbial diversity. *Nature*, 551(7681), 457–463. doi: 10.1038/nature24621

Tinta, T., Kogovšek, T., Klun, K., Malej, A., Herndl, G. J., & Turk, V. (2019). Jellyfish-associated microbiome in the marine environment: exploring its biotechnological potential. *Marine Drugs*, 17(2). doi: 10.3390/md17020094

Turner, J. T. (2015). Zooplankton fecal pellets, marine snow, phytodetritus and the ocean's biological pump. *Progress in Oceanography*, 130, 205–248. doi: 10.1016/j.pocean.2014.08.005

Vargas, C. A., & Madin, L. P. (2004). Zooplankton feeding ecology: clearance and ingestion rates of the salps *Thalia democratica*, *Cyclosalpa affinis* and *Salpa cylindrica* on naturally occurring particles in the Mid-Atlantic Bight. *Journal of Plankton Research*, 26(7), 827–833. doi: 10.1093/plankt/fbh068

Vergin, K. L., Beszteri, B., Monier, A., Cameron Thrash, J., Temperton, B., Treusch, A. H., ... Giovannoni, S. J. (2013). High-resolution SAR11 ecotype dynamics at the Bermuda Atlantic Time-series Study site by phylogenetic placement of pyrosequences. *The ISME Journal*, 7(7), 1322–1332. doi: 10.1038/ismej.2013.32

Viver, T., Orellana, L. H., Hatt, J. K., Urdiain, M., Díaz, S., Richter, M., ... Rosselló-Móra, R. (2017). The low diverse gastric microbiome of the jellyfish *Cotylorhiza tuberculata* is dominated by four novel taxa. *Environmental Microbiology*, 19(8), 3039–3058. doi: 10.1111/1462-2920.13763

Voogd, N. J. de, de Voogd, N. J., Cleary, D. F. R., Polónia, A. R. M., & Gomes, N. C. M. (2015). Bacterial community composition and predicted functional ecology of sponges, sediment and seawater from the thousand islands reef complex, West Java, Indonesia. *FEMS Microbiology Ecology*, 91(4). doi: 10.1093/fem-sec/fiv019

Walters, T. L., Lamboley, L. M., López-Figueroa, N. B., Rodríguez-Santiago, Á. E., Gibson, D. M., & Frischer, M. E. (2019). Diet and trophic interactions of a circumglobally significant gelatinous marine zoo-plankter, *Dolioletta gegenbauri* (Uljanin, 1884). *Molecular Ecology*, 28(2), 176–189. doi: 10.1111/mec.14926

Wickham, H. (2016).ggplot2: Elegant graphics for data analysis. Springer.

Winder, M., Bouquet, J.-M., Rafael Bermúdez, J., Berger, S. A., Hansen, T., Brandes, J., ... Thompson, E. M. (2017). Increased appendicularian zooplankton alter carbon cycling under warmer more acidified ocean conditions. *Limnology and Oceanography*, 62(4), 1541–1551. doi: 10.1002/lno.10516

Yeh, H. D., Questel, J. M., Maas, K. R., & Bucklin, A. (2020). Metabarcoding analysis of regional variation in gut contents of the copepod *Calanus finmarchicus* in the North Atlantic Ocean. *Deep-Sea Research. Part II, Topical Studies in Oceanography*, 180, 104738. doi: 10.1016/j.dsr2.2020.104738

Yilmaz, P., Yarza, P., Rapp, J. Z., & Glöckner, F. O. (2015). Expanding the world of marine bacterial and archaeal clades. *Frontiers in Microbiology*, *6*, 1524. doi: 10.3389/fmicb.2015.01524

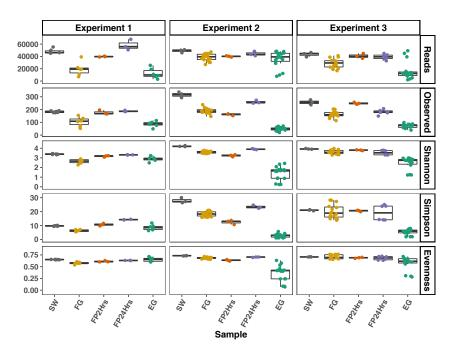
Yuan, H., Li, T., Li, H., Wang, C., Li, L., Lin, X., & Lin, S. (2021). Diversity distribution, driving factors and assembly mechanisms of free-living and particle-associated bacterial communities at a subtropical marginal sea. *Microorganisms*, 9(12). doi: 10.3390/microorganisms9122445

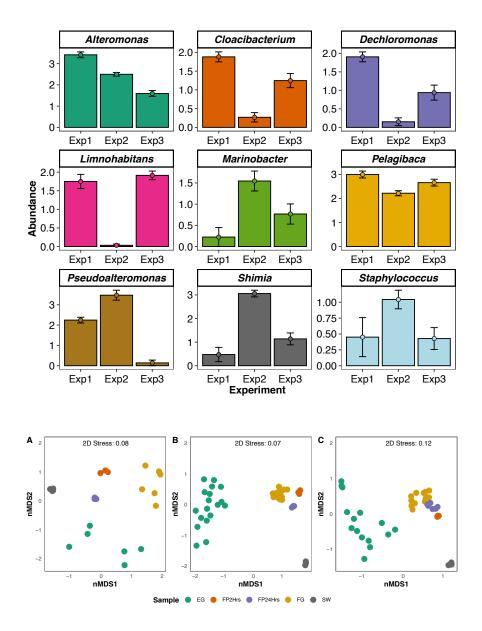
Zamora-Terol, S., Novotny, A., & Winder, M. (2020). Reconstructing marine plankton food web interactions using DNA metabarcoding. *Molecular Ecology*, 29(17), 3380–3395. doi: 10.1111/mec.15555

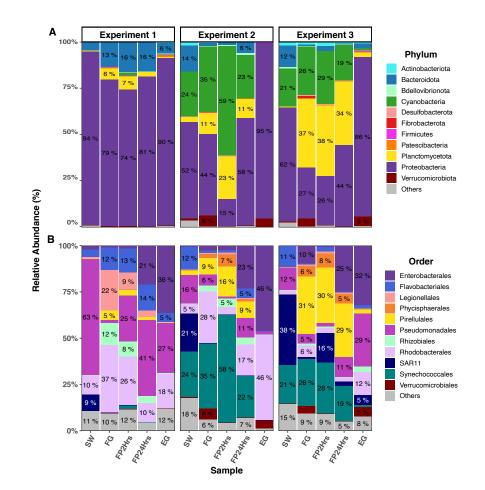
Zar, J. H. (2010). Biostatistical analysis (5th ed.). Prentice-Hall/Pearson.

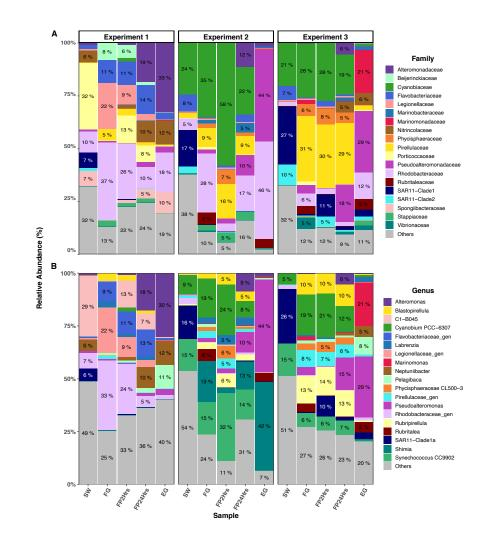
Hosted file

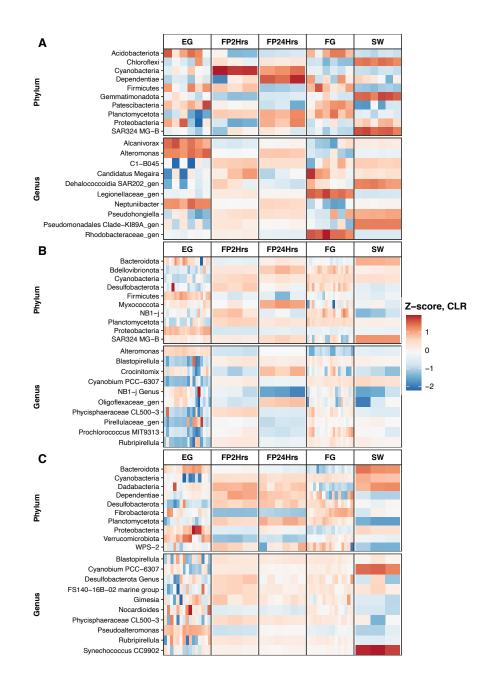
Table 1.docx available at https://authorea.com/users/455406/articles/552723-the-microbiomeof-the-pelagic-tunicate-dolioletta-gegenbauri-a-potential-link-between-the-grazing-andmicrobial-food-web











Α			EG		FP2Hrs	FP24Hrs	FG	SW		
	5-dehydro-4-deoxy-D-glucuronate isomerase -									
	5-guanidino-2-oxopentanoate decarboxylase -									
5-methyltetra	ahydropteroyltriglutamatehomocysteine S-methyltransferase -			_						
	Acetoacetate decarboxylase -									
	Alanine transaminase -	1								
	Carboxynorspermidine decarboxylase - Enoyl-[acyl-carrier-protein] reductase -									
	Glycerate 3-kinase		Υ.							
E.	Homoserine O-acetyltransferase -		0				12			
đ	L-gulonolactone oxidase									
Ā	Nicotinamide phosphoribosyltransferase -									
EC Number	Protein disulfide-isomerase -						10			
ш	Pseudolysin -		n							
	Serralysin -									
	Sulfopyruvate decarboxylase -									
	Tellurite methyltransferase -									
	Tubulintyrosine ligase -									
	Uronate dehydrogenase -									
	Valinepyruvate transaminase -									
	Xaa-Pro dipeptidase -									
в			EG	i	FP2Hrs	FP24Hrs	F	G	SW	
	"6,7-dimethyl-8-ribityllumazine synthase" -									
	Acid phosphatase -		а.							
	Adenylate kinase - All-trans-zeta-carotene desaturase -									
	Alpha-methylacyl-CoA racemase -			11						
	Cadmium-exporting ATPase	÷.	1							Z-score, CLR
	Calcium-transporting ATPase -	10	Π.	10						
_	Coenzyme F420 hydrogenase -									1
£:	Divinyl chlorophyllide a 8-vinyl-reductase -									
ų.	dTMP kinase -		ш							0
EC description	Ferroxidase -									-1
ð	GDP-perosamine synthase - GlutamatetRNA ligase -									
	Isocitrate dehydrogenase (NADP(+)) -									2
	Lycopene epsilon-cyclase									3
	N-acetylmuramoyl-L-alanine amidase -									-
	Phytoene desaturase (lycopene-forming) -		Ш							
	Protein-disulfide reductase -									
	Thiamine-phosphate diphosphorylase -									
	Xaa-Pro dipeptidase -		U.							
	Zinc-exporting ATPase -									
С			EG	i	FP2Hrs	FP24Hrs	F	G	SW	
	"Tryptophan 2,3-dioxygenase" -									
	16S rRNA (guanine(1207)–N(2))–methyltransferase -									
	3-deoxy-D-manno-octulosonic acid kinase -									
	3-deoxy-D-manno-octulosonic acid kinase - 3-oxoacid CoA-transferase -									
	3-deoxy-D-manno-octulosonic acid kinase 3-oxoacid CoA-transferase Adenosylcobalamin/alpha-ribazole phosphatase									
	3-deoxy-D-manno-octulosonic acid kinase 3-oxoacid CoA-transferase Adenosylcobalamin/alpha-ribazole phosphatase Assimilatory sulfite reductase (NADPH)									
c	3-deoxy-D-manno-octulosonic acid kinase 3-oxoacid CoA-transferase Adenosylcobalamin/alpha-ribazole phosphatase Assimilatory sulfite reductase (NADPH) Dihydrolipoyllysine-residue (2-methylpropanoyl)transferase									
tion	3-deoxy-D-manno-octulosonic acid kinase 3-oxoacid OoA-transferase Adenosylcobalamirlalpha-ribazole phosphatase Assimilatory sulfite reductase (NADPH) Dihydrolipoyllysine-residue (2-methylpropanoyl)transferase Forminidoylglutamase									
ription	3-deoxy-D-manno-octulosonic acid kinase 3-oxoacid CoA-transferase Adenosyloobalasni/alpha-ribazole phosphatase Assimilatory sulfite reductase (NADPH) Dihydrolipoyllysine-residue (2-methylpropanoy)/transferase Formimidoylglutamase Gamma-glutamyl hercynylcysteine S-oxide hydrolase									
scription	3-deoxy-D-manno-octulosonic acid kinase 3-oxoacid CoA-transferase Adenosylcobalamiin/alpha-ribazole phosphatase Assimilatory sulfite reductase (NADPH) Dihydrolipoyllysine-residue (2-methytpropanoyl)transferase Formimidoylglutamase Gamma-glutamyl hercynylcysteine S-oxide hydrolase Glucosamine kinase									
description	3-deoxy-D-manno-octulosonic acid kinase 3-oxoacid CoA-transferase Adenosylcobalamin/alpha-ribazole phosphatase Assimilatory sulfite reductase (NADPH) Dihydrolipoyllysine-residue (2-methylpropanoyl)transferase Formimidoylglutamase Gamma-glutamyl hercynylcysteine S-oxide hydrolase Glucose-6-phosphate 1-epimerase									
EC description	3-deoxy-D-manno-octulosonic acid kinase 3-oxoacid CoA-transferase Adenosyloobalami/alpha-ribazole phosphatase Assimilatory sulfite reductase (NADPH) Dihydrolipoyllysine-residue (2-methylpropanoy)/transferase Formimidoylglutamase Gamma-glutamyl hercynylcysteine S-oxide hydrolase Glucosamine kinase Glucose-6-phosphate 1-epimerase Maleylpyruvate isomerase									
EC description	3-deoxy-D-manno-octulosonic acid kinase 3-oxoacid CoA-transferase Adenosylcobalamiin/alpha-ribazole phosphatase Assimilatory sulfite reductase (NADPH) Dihydrolipoyllysine-residue (2-methylpropanoyl)transferase Formimidoylgutamase Gamma-glutamyl hercynylcysteine S-oxide hydrolase Glucose-B-phosphate 1-epimerase Maleylpyruvate isomerase N-hydroxyarylamine O-acetyltransferase									
EC description	3-deoxy-D-manno-octulosonic acid kinase 3-oxoacid CoA-transferase Adenosyloobalami/alpha-ribazole phosphatase Assimilatory sulfite reductase (NADPH) Dihydrolipoyllysine-residue (2-methylpropanoy)/transferase Formimidoylglutamase Gamma-glutamyl hercynylcysteine S-oxide hydrolase Glucosamine kinase Glucose-6-phosphate 1-epimerase Maleylpyruvate isomerase									
EC description	3-deoxy-D-manno-octulosonic acid kinase 3-oxoacid CoA-transferase Adenosylcobalamin/alpha-ribazole phosphatase Assimilatory sulfite reductase (NADPH) Dihydrolipoyllysine-residue (2-methylpropanoyl)transferase Forminidoylglutamase Gamma-glutamyl hercynylcysteine S-oxide hydrolase Glucose-6-phosphate 1-epimerase Maleylpyruvate isomerase N-hydroxyarylamine O-acetyltransferase Phosphogluconate dehydratase									
EC description	3-deoxy-D-manno-octulosonic acid kinase 3-oxoacid CoA-transferase Adenosylcobalamin/alpha-ribazole phosphatase Assimilatory suffite reductase (NADPH) Dihydrolipoyllysine-residue (2-methylpropanoyl)transferase Formimidoylglutamase Gamma-glutamyl hercynylcysteine S-oxide hydrolase Glucosamine kinase Glucosamine kinase Algelypruzate isomerese Małę/pyruzate isomerese N-hydroxyarylamine O-acetyltransferase Phosphogluconate dehydratase Phospholipase A(1)									
EC description	3-deoxy-D-manno-octulosonic acid kinase 3-oxoacid CoA-transferase Adenosylcobalamiin/alpha-ribazole phosphatase Assimilatory sulfite reductase (NADPH) Dihydrolipoyllysine-residue (2-methylpropanoyl)transferase Formimidoylgiutamase Gamma-glutamyl hercynylcysteine S-oxide hydrolase Glucosen-6-phosphate 1-epimerase Maleylpyruvate isomerase N-hydroxyarylamine O-acetyltransferase Phosphogluconate dehydratase Phospholipase A(1)									
EC description	3-deoxy-D-manno-octulosonic acid kinase 3-oxoacid CoA-transferase Adenosylcobalami/alpha-ribazole phosphatase Assimilatory sulfite reductase (NADPH) Dihydrolipoyllysine-residue (2-methylpropanoy)/transferase Formimidoylgutamase Gamma-glutamyl hercynylcysteine S-oxide hydrolase Glucose-6-phosphate 1-epimerase Maleyloyruxate isomerase N-hydroxyarylamine O-acetyltransferase Phospholipase A(1) Phospholipase A(2) Protein disulfide-isomerase									